Geochimica et Cosmochimica Acta
August 2015, Volume 162, Pages 66-82
http://dx.doi.org/10.1016/j.gca.2015.04.031
http://archimer.ifremer.fr/doc/00266/37715/

Total dissolvable and dissolved iron isotopes in the water column of the Peru upwelling regime

Chever Fanny [1, 2, *], Rouxel Olivier [3], Croot Peter L. [4, 5, 6], Ponzevera Emmanuel [3], Wuttig Kathrin [4], Auro Maureen [7]

[1] Institut Universitaire Européen de la Mer, Université de Bretagne Occidentale, 29280 Plouzané, France
[2] IFREMER, Centre de Brest, Département REM/EEP/Laboratoire Environnement Profond, CS 10070, 29280 Plouzané, France
[3] IFREMER, Centre de Brest, Département REM/EEP/Laboratoire Environnement Profond, CS 10070, 29280 Plouzané, France
[4] GEOMAR Helmholtz Centre for Ocean Research Kiel, Marine Biogeochemistry, Düsternbrooker Weg 20, 24105 Kiel, Germany
[5] Plymouth Marine Laboratory (PML), Plymouth, Devon, United Kingdom
[6] Earth and Ocean Sciences, School of Natural Sciences, National University of Ireland, Galway, University Road, Galway, Ireland
[7] Department of Marine Chemistry and Geochemistry, Woods Hole Oceanographic Institute, Woods Hole, MA 02543, USA

* Corresponding author : Fanny Chever, Tel.: +33 2 98 22 45 24. ;
email address : Fanny.Chever@ifremer.fr

Abstract :

Vertical distributions of iron (Fe) concentrations and isotopes were determined in the total dissolvable and dissolved pools in the water column at three coastal stations located along the Peruvian margin, in the core of the Oxygen Minimum Zone (OMZ). The shallowest station 121 (161 m total water depth) was characterized by lithogenic input from the continental plateau, yielding concentrations as high as 456 nM in the total dissolvable pool. At the 2 other stations (stations 122 and 123), Fe concentrations of dissolved and total dissolvable pools exhibited maxima in both surface and deep layers. Fe isotopic composition (δ56Fe) showed a fractionation toward lighter values for both physical pools throughout the water column for all stations with minimum values observed for the surface layer (between -0.64 and -0.97 ‰ at 10 - 20 m depth) and deep layer (between -0.03 to -1.25 ‰ at 160 - 300 m depth). An Fe isotope budget was established to determine the isotopic composition of the particulate pool. We observed a range of δ56Fe values for particulate Fe from + 0.02 to -0.87 ‰, with lightest values obtained at water depth above 50 m. Such light values in the both particulate and dissolved pools suggest sources other than atmospheric dust deposition in the surface ocean, including lateral transport of isotopically light Fe. Samples collected at station 122 closest to the sediment show the lightest isotope composition in the dissolved and the particulate pools (-1.25 and -0.53 ‰ respectively) and high Fe(II) concentrations (14.2 ± 2.1 nM) consistent with a major reductive benthic Fe sources that is transferred to the ocean water column. A simple isotopic model is proposed to link the extent of Fe(II) oxidation and the Fe isotope composition of both particulate and dissolved Fe pools. This study

demonstrates that Fe isotopic composition in OMZ regions is not only affected by the relative contribution of reductive and non-reductive shelf sediment input but also by seawater-column processes during the transport and oxidation of Fe from the source region to open seawater.

Keywords : Iron isotopes, Peru Margin, Iron redox cycle, Benthic source

1. Introduction

Iron (Fe) is an essential micronutrient for marine organisms (Martin and Fitzwater 1988). It is now well established that this element plays a key role in the functioning of the marine ecosystems (Moore et al. 2002; Boyd and Ellwood 2010). *In-situ* and natural Fe fertilisations have demonstrated that Fe inputs enhance phytoplankton biomass and affect the major biogeochemical cycles (e.g. carbon (C) and nitrogen (N)) (Boyd et al. 2000; Coale et al. 2004; Jickells et al. 2005; Blain et al. 2007; Boyd et al. 2007; Pollard et al. 2009). However, the importance of new and regenerated sources of Fe to the water column as well as the fractions that are truly bioavailable to the phytoplankton, are still subject of debate.

Whereas atmospheric deposition was commonly thought to be the predominant external source of Fe in remote areas (Jickells et al. 2005), inputs from sediments coupled to upwelling or advection are now considered to provide significant supply of Fe to surface waters of the open ocean (Bucciarelli et al. 2001; Elrod et al. 2004; Lam and Bishop 2008; Tagliabue et al. 2009; Nishioka et al. 2011). In contrast to the open ocean, shelf environments may receive additional Fe input from fluvial sources and sediment resuspension (Croot and Hunter 1998; Hutchins and Bruland 1998; Johnson et al. 2001; Elrod et al. 2004; Lam and Bishop 2008; Lohan and Bruland 2008). Even if Fe supply is significant in those regions, some studies have shown that, due to the complex physico-chemical speciation of Fe in coastal systems, its bioavailability can be limited (Hutchins and Bruland 1998).

In seawater, Fe occurs in two redox states, Fe(II) and Fe(III) (Waite and Morel 1984). In oxic seawater, the thermodynamically stable state Fe(III) is highly insoluble (Liu and Millero 2002) and rapidly hydrolyzes resulting in the precipitation of various Fe(III) oxyhydroxides. Organic ligands complex most of the dissolved Fe in seawater and control the solubility of Fe(III) (Gledhill and van den Berg 1994; Rue and Bruland 1995; Millero 1998; Barbeau et al. 2001; Liu and Millero 2002; Gledhill and Buck 2012). Fe(II) is more soluble but is rapidly oxidized by oxygen (O_2) and hydrogen peroxide (H_2O_2) (Millero et al. 1987; Millero and Sotolongo 1989; Gonzalez-Davila et al. 2005; Santana-Casiano et al. 2005; Sarthou et al. 2011). Reduction of Fe(III) to Fe(II) with possible stabilization by organic ligands is a potential mechanism by which Fe is made more bioavailable to phytoplankton (Anderson and Morel 1980; Maldonado and Price 2001). The release of Fe(II) from reducing continental-margin sediments (Hong and Kester 1986; Lohan and Bruland 2008) as well as Fe(II) supply from seafloor hydrothermal vents (Bennett et al. 2008; Toner et al. 2009; Tagliabue et al. 2010; Wu et al. 2011a; Nishioka et al. 2013; Vedamati et al. 2014) are now

recognized as possible sources of Fe(II) in seawater. Under anoxic conditions as those encountered in relatively organic-rich marine sediments, when sulfide generation is limited and thus precluding the precipitation of FeS minerals reductive dissolution of Fe oxides or clay minerals can result in dissolved Fe(II) concentrations up to 1 mM (Sell and Morse 2006). In open ocean surface waters, the photoreduction of Fe(III) to Fe(II) has also been clearly observed (Croot et al. 2008).

The Peruvian coast is characterized by an intensive mid-depth region of low oxygen associated with an upwelling and high surface productivity (Hong and Kester 1986; Bruland et al. 2005; Stramma et al. 2010). Major changes to marine sources and sinks of important nutrients such as nitrogen, phosphorus and Fe occur when oceanic oxygen concentrations decrease below threshold levels (Stramma et al. 2008). Along the continental shelf off the Peruvian coast, labile Fe (i.e. Fe(II)) concentrations up to 73 nM were attributed to intense redox cycling occurring at the sediment-water interface (Hong and Kester 1986; Vedamati et al. 2014). This process can result in a greatly enhanced source of Fe available to upwell to surface waters, potentially increasing phytoplankton productivity (Lohan and Bruland 2008). The Oxygen Minimum Zones (OMZs) of the tropics are key regions of low oxygen in today's ocean. The effects of nutrient cycling under oxygen deficient conditions are carried into the rest of the ocean by the thermohaline circulation (Stramma et al. 2008). Hence processes occurring in the OMZs, impacting nutrients and Fe cycles, may have an impact on the biological productivity and carbon cycle of the global ocean (Helly and Levin 2004; Pennington et al. 2006). Given the fact that expansion of the OMZs will continue to occur in the future (Stramma et al. 2008), a better understanding of Fe biogeochemical cycle in those environments is of great interest.

Recent studies of Fe isotopes in open seawater and coastal regions have shown variability in δ^{56}Fe and have demonstrated how Fe isotopes may be used to constrain the global Fe cycle. The Fe isotope composition is expressed by δ^{56}Fe defined as:

$$\delta^{56}Fe = \left[\frac{(^{56}Fe/^{54}Fe)_{sample}}{(^{56}Fe/^{54}Fe)_{IRMM-14}} - 1 \right] \times 10^{3}$$. Values are reported relative to the IRMM-14 international iron isotope reference material (the δ^{56}Fe of igneous rocks relative to IRMM is of +0.09 ± 0.1 ‰, 2SD; Beard et al. 2003a).

In nature, δ^{56}Fe variations are mainly controlled by both biotic and abiotic redox processes along with a range of isotope (kinetic and/or equilibrium) fractionations arising from non-redox processes (e.g. Welch et al. 2003; Croal et al. 2004; Johnson et al. 2004;

Balci et al. 2006; Dauphas and Rouxel 2006). Numerous studies were initially led at the ocean boundaries to characterize Fe sources to the ocean such as aerosols, sediment porewaters, groundwaters, rivers and hydrothermal vents (Sharma et al. 2001; Severmann et al. 2004; Bergquist and Boyle 2006; Severmann et al. 2006; Rouxel et al. 2008a; Rouxel et al. 2008b; Bennett et al. 2009; Escoube et al. 2009; Homoky et al. 2009; Severmann et al. 2010; Roy et al. 2012). Those studies demonstrated that benthic sources of Fe are often characterized with light isotopic values. In the case of benthic input from reducing sediments, Fe isotope composition of pore-fluid at the sediment-seawater interface is highly sensitive to local redox conditions, with most light δ^{56}Fe values being generated through the combination of microbial Fe reduction and partial Fe oxidation (Severmann et al., 2006; Homoky et al., 2009). Heavy δ^{56}Fe values have been also found in anoxic sediment porewater as a result of the development of sulfidic conditions and the precipitation of isotopically light Fe sulfides (Severmann et al. 2006; Roy et al. 2012). Homoky et al. (2013) recently highlighted the importance of the 'non-reductive' dissolution of continental margin sediments as a source of dissolved Fe in seawater that is characterized by δ^{56}Fe values close to crustal values.

The isotopic composition of dissolved Fe in seawater has received much interest in recent years (Lacan et al. 2008; John and Adkins 2010; Lacan et al. 2010; Rouxel and Auro 2010; Radic et al. 2011; Boyle et al. 2012; John et al. 2012; Conway and John 2014). Radic et al. (2011) reported Fe isotope values for open ocean seawater from the equatorial Pacific. Dissolved Fe (DFe) concentrations ranged from 0.1 to 1.5 nM, yielding δ^{56}Fe values of +0.01 - +0.58 ‰ whereas particulate Fe (PFe) concentrations ranged from 0.4 nM to 32.2 nM with similar range of δ^{56}Fe values between -0.02 to +0.46 ‰. These values compare well with other Fe isotope results from the South-eastern Atlantic with, $\delta^{56}Fe_{DFe}$ = -0.14 to +0.23 ‰ (Lacan et al. 2008) and from the North Atlantic near Bermuda with $\delta^{56}Fe_{DFe}$ = +0.30 to +0.71 ‰ (John et al. 2012). In contrast, light $\delta^{56}Fe_{DFe}$ values from -1.82 to 0.00 ‰ have been reported in the San Pedro Basin and from -3.45 to -0.29 ‰ in the Santa Barbara basins (John et al. 2012). In both basins, the lowest $\delta^{56}Fe_{DFe}$ values and highest Fe concentrations are found at the bottom of the basin reflecting the input of isotopically light Fe from reducing sediment porewaters. Coastal seawater values also display a range of $\delta^{56}Fe_{DFe}$ values reflecting mainly the relative contribution of benthic vs. riverine Fe sources (Rouxel and Auro 2010).

Recently, Conway and John (2014) reported a high-resolution transect of $\delta^{56}Fe_{DFe}$ values along a section of the North Atlantic Ocean. This study allowed a first-order assessment of the potential contribution of different Fe sources to the ocean, such as Fe derived from dust dissolution ($\delta^{56}Fe_{DFe}$ as high as +0.68 ‰), Fe released through reductive

and non-reductive sedimentary dissolution ($\delta^{56}Fe_{DFe}$ estimated as -2.4 and +0.09 ‰, respectively), and Fe from seafloor hydrothermal plumes ($\delta^{56}Fe_{DFe}$ estimated as -1.35 ‰). This mass balance approach, however, implies that the Fe isotope signatures of the different Fe sources are well characterized and conservative during oceanic mixing.

Hence despite the recent progress in our understanding of Fe isotope systematics in marine environments, we still do not fully understand how the biogeochemical processes occurring in the water column affect the Fe isotope composition. Here, the aim of this study is to provide further constraints on the range of Fe isotope compositions in a shelf environment featuring a prominent OMZ. Through a combined approach linking Fe speciation and Fe isotope data, we aim to (1) determine the end-member Fe isotopic value of Fe(II) derived from reductive dissolution of sediments and being released in the water column; (2) test the hypothesis that the isotopic composition of the reductive benthic Fe flux is controlled by water column processes that modify its initial source composition.

In this paper, we present the concentration and isotopic composition of Fe in the total dissolvable and dissolved pools in the water column from three stations located along the Peruvian coast, in the core of the OMZ. Those values are discussed with regard to Fe(II) concentrations that were measured on-board. To our knowledge this study is the first to report a vertical profile of $\delta^{56}Fe$ (in both dissolved and total pools) combined with redox speciation (with the measurement of Fe(II) concentrations). This study provides an excellent opportunity to investigate Fe isotope systematics in oxygen-depleted shelf setting where intense redox cycling occurs at the sediment/water interface.

2. Study area and sampling strategy

The METEOR cruise leg M77/4 took place in January-February 2009 in the South-eastern tropical Pacific (**Fig. 1**). Hydrocast samplings were performed using the shipboard CTD rosette equipped with standard 12 L Niskin bottles for stations 121 and 122 whereas 8 L Teflon lined Go-Flo bottles mounted on a trace metal clean hydrowire were used for station 123. Samples were collected in acid-cleaned bottles following GEOTRACES protocols (Bruland et al. 1979; Cutter et al. 2010; Boyle et al. 2012). Sampling was carried out in a purpose built class 100 shipboard clean container (Clean Modules, UK) owned by GEOMAR. All samples were collected in 1 L acid-washed low density polyethylene (LDPE) bottles. Total dissolvable Fe (TDFe) was sampled directly without any filtration steps. Samples for DFe were obtained from the bottles by slight over pressure (0.2 bar) with high-purity nitrogen

to allow online filtration of seawater through 0.2 µm cartridge filters (SARTOBAN®). All samples were acidified on board to pH ~ 1.8 with Optima-grade hydrochloric acid (HCl) in an iso class 5 clean laboratory. The samples were then stored at room temperature for more than 12 months before analysis at WHOI or IFREMER laboratories.

Samples for Fe(II) were collected during the same Niskin/GO-Flo casts as the DFe and TDFe samplings. Immediately upon recovery of the bottles, samples were collected without any filtration in acid-cleaned 125 mL amber HDPE bottles. Hence, the potential entrainment of Fe(II) bearing particles (e.g. from Fe sulfides or clays), especially at near-shore stations, cannot be excluded. In practice we have found no difference between filtered and unfiltered samples for Fe(II) concentrations for open ocean waters (Croot and Heller 2012) suggesting minimal contribution of Fe(II) from marine particles there. Oxygen concentrations reported in **Fig. 2** were determined using Winkler titration (Hansen 1999) in water sampled from Niskin bottles deployed at the same location and depth as the Go-Flo bottles (detection limit = 3 µM O_2, 3 SD).

In this study, we selected 3 stations located along the Peruvian shelf between 5°S and 6°S (stations 121, 122 and 123), in the OMZ (**Fig. 1**). Stations 121 and 122 are shallow stations, with a bottom depth of 161 and 199 m, respectively. In contrast, station 123, located offshore, has a water depth of 2430 m. Seawater samples were collected from the surface (10 m at stations 121 and 122, 20 m at station 123) to the bottom water at stations 121 and 122 (160 and 193 m, respectively) and up to 300 m depth at station 123. Hence, sampling at station 123 did not include a full depth profile to provide the same depth range as the shallow on-shore stations. This approach, however, is sufficient to discuss evidences of any off-shore advection of Fe within the OMZ. The water column was sampled for TDFe at all stations, and for DFe at stations 122 and 123, for the determination of Fe concentration and isotopic composition. Samples for Fe(II) concentrations were also collected and analyzed in near real time at those three stations.

3. Analytical Method

3.1. Iron concentrations

TDFe and DFe concentrations and isotope compositions presented in this paper (**Table 1**) were determined using the same sample aliquot on a Neptune (Thermo Scientific) multi-

collector inductively coupled plasma mass spectrometer (MC-ICPMS). In short, the purified samples collected after passing through nitrilotriacetic acid functional groups (NTA, Qiagen Inc., Valencia, CA) and AG1-X8 resins (see below), were diluted 10-fold and measured against calibrated standard solutions. This technique, which has been previously used to measure Fe concentration and isotope composition in coastal and open seawater (Rouxel and Auro, 2010; John and Adkins, 2010), allows a precision of ~10% (1SD) on the concentrations. The relatively larger uncertainty compared to other methods using isotope dilution (e.g. Lacan et al., 2010; Conway and John, 2014) is mainly due to dilution errors and extraction efficiency of the NTA resin ranging from 95 to 100%. The accuracy of the methods has been further assessed both through standard addition experiments and the analysis of certified seawater standards (Rouxel and Auro, 2010). The detection limit has been assessed to be 0.05 nM. Fe(II) samples were analyzed using a chemiluminescence flow injection analysis system following the same method as Croot et al. (2008) and will be discussed more in detail in a separate paper. Total dissolvable particulate Fe is calculated by subtracting the 0.2 µm filtered fraction (DFe) from the unfiltered one (TDFe). It is expressed as PFe and data are reported in **Table 1**. It should be noted that some very refractory lithogenic or crystalline Fe particles remain unreactive to the TDFe mild acid leaching (Bowie et al. 2010), and thus PFe does not represent the entire particulate Fe pool.

3.2. Iron isotope analysis

Samples were first pre-concentrated onto a NTA resin following the same method as (Rouxel and Auro 2010) and (Boyle et al. 2012). This method has already been successfully used by many laboratories (John and Adkins 2010; Lacan et al. 2010; Boyle et al. 2012) due to its specificity for Fe (Lohan et al. 2005), allowing it to attain complete recovery of Fe from large volumes of acidified seawater. Briefly, before sample processing though NTA resin, the pH of each sample was checked and adjusted using ultra-clean HCl (optima grade, Fisher) to obtain a pH between 1.7 and 1.8. Hydrogen peroxide (30% v/v Optima grade, Fisher) was then added to a concentration of 1 mL/L to oxidize any ferrous Fe present in the sample prior to sample processing. The NTA resin was packed into acid-cleaned chromatographic columns (Poly-Prep columns, Bio-Rad Inc.) with a wet volume of 1.8 mL. Prior to sample loading, the resin was resuspended and rinsed with 25 mL of a 0.7 M nitric acid (HNO_3) + 0.6 M HCl mixture followed by 50 mL of 18.2 MΩ.cm purified water acidified to pH 1.8 with ultra-clean HCl. Between 900 and 950 mL of water sample were passed through the NTA chromatographic columns and the remaining volume was archived. A peristaltic pump

operating at a constant flow rate between 2.5 to 5 mL/min was used to slowly draw the samples through the chromatographic columns. After the water sample was passed through the resin, 15 mL of pH 1.8 Milli-Q water was used to elute the remaining sample matrix from the column walls and resin. Fe was finally eluted with 7 mL of 1.4 M HNO_3, recovered in acid-cleaned 8 mL polytetrafluoroethylene (PTFE) vials and evaporated on an all-Teflon hot plate. Evaporated samples were then redissolved in 6 M HCl for further purification through AG1-X8 (Bio-Rad, Inc.) anion resin following previously established methods (e.g. Escoube et al., 2009; Rouxel et al., 2008b).

Analyzes of $^{56}Fe/^{54}Fe$ and $^{57}Fe/^{54}Fe$ ratios were carried out using a Thermo Scientific Neptune MC-ICP-MS at IFREMER (Brest, France). The medium mass resolution mode was used to resolve isobaric interferences, such as $^{40}Ar^{16}O^{+}$ on $^{56}Fe^{+}$, $^{40}Ar^{16}O^{1}H^{+}$ on $^{57}Fe^{+}$, and $^{40}Ar^{14}N^{+}$ on $^{54}Fe^{+}$ (Weyer and Schwieters 2003). Two blocks of 25 integrations of 4 s were measured. Samples were introduced into the plasma torch using an Apex-Q introduction system (Elemental Scientific) and a PFA micro-concentric nebulizer operating at a flow rate of about 60 µl. min^{-1}. The Apex-Q system increases the instrument sensitivity by a factor of 5 relative to conventional spray chambers. The instrument sensitivity was further improved using X-cones which resulted in a ~2-fold increase of instrument sensitivity relative to normal cones. ^{54}Fe, ^{56}Fe, ^{57}Fe, ^{60}Ni and ^{62}Ni isotope signals were acquired simultaneously on Faraday cups. Baseline corrections were made before acquisition of each data block by completely deflecting the ion beam. Although separated, isobaric Cr interference was always checked and corrected during all analysis, using the Neptune's peak jumping mode on ^{52}Cr mass. A standard bracketing approach, which normalizes the Fe isotope ratio to the average measured composition of a standard (IRMM-14) was carried out before and after each sample. All sample and standard solutions were diluted with 0.28 M ultra-clean HNO3 (Optima Grade, Fisher) in appropriate concentrations so that the bracketing standard (i.e. IRMM-14) had approximately the same concentration as the sample (± 10 %). Instrumental mass bias was corrected using an internal Ni standard (SRM 986). The two methods combined permit higher precision and the verification of any instrumental artefacts generated by residual matrix elements. The internal precision of the data at 95 % confidence levels reported in **Table 1** were calculated based on the analysis of the bracketing standards. Analyses were carried out using 2-3 mL of Fe solutions. The pure IRMM-14 standard gave a $\delta^{56}Fe$ external precision of 0.04 to 0.13 ‰ (2σ) for Fe concentrations ranging from 400 to 70 ppb, respectively. We also used an internal Fe standard provided by NIST (SRM3126a) which yielded $\delta^{56}Fe$ values of +0.42 ± 0.07 ‰ (2σ, n=10) relative to IRMM-14. This value is indistinguishable, within

uncertainty, from its nominal $\delta^{56}Fe$ value of +0.39 ‰ (Rouxel and Auro, 2010). This standard is used as external control of instrumental accuracy and is used routinely throughout the entire chemical purification procedure. We also measured $\delta^{57}Fe$ values, but the values are generally less precise due to lower ^{57}Fe abundances relative to ^{56}Fe. Since the relationship between $\delta^{56}Fe$ and $\delta^{57}Fe$ of the samples plots on a mass fractionation line, only $\delta^{56}Fe$ values are discussed in this paper.

4. Results

4.1. Hydrography

The temperature-salinity (T-S) diagram for the depths sampled for Fe analysis is plotted in **Fig. 2a**. The three stations are composed of the same water masses, with a mixing of a surface layer (S > 35.0 and T > 15 °C) with a deeper water mass (S < 34.7 and T < 10 °C). Potential differences observed between the vertical profiles cannot thus be explained by differences in water masses.

Surface waters are characterized by dissolved oxygen concentrations ranging from 57 µM (station 121) to 225 µM (station 123) (**Fig. 2b**). Below the surface layer, O_2 concentrations decrease sharply, reaching hypoxic concentrations at just 10 m depth at stations 121 and 122 (23 and 35 µM) and at 70 m at station 123 (11 µM). Bottom water O_2 concentrations of 23 and 4 µM were observed at stations 121 and 122, respectively. At the offshore station 123, O_2 concentration rapidly decreased to concentrations < 10 µM below 40 m, reaching a minimum of 5 µM at 300 m depth. In previous study areas of benthic Fe supply led along the California Borderland Basins, similarly low bottom O_2 concentration of 3 - 4 µM have been already reported (Severmann et al. 2010). In the same area as ours, Hong and Kester (1986) and Noffke et al. (2012) also observed vertical O_2 concentrations decreasing from more than 200 to less than 10 µM from the surface to the bottom waters. By comparison, in the hypoxic shelf waters off Oregon and Washington, Lohan and Bruland (2008) observed a minimum oxygen concentration of 43 µM within the bottom boundary layer whereas Severmann et al. (2010) measured bottom water oxygen concentrations ranging between 30 and 50 µM along the southern Oregon coast.

4.2. Vertical distribution of Fe and $\delta^{56}Fe$

Iron concentrations

Vertical distributions of Fe are plotted in **Fig. 3,** while concentrations are reported in **Table 1**. In the total dissolvable pool, the highest concentrations were observed at station 121. At this station, TDFe (**Fig. 3a**) concentrations increased from the surface to 100 m (with values ranging from 14.6 nM to 456 nM) before decreasing to a bottom concentration of 200 nM at 160 m. At stations 122 and 123, a maximum of TDFe was observed in the surface layer with values of 32.9 nM and 14.3 nM, respectively and a minimum was reached for both stations at 50 m (TDFe of 7.3 and 3.7 nM at stations 122 and 123 respectively). Concentrations increased then with depth. At the station 122, TDFe concentrations reached 61.8 ± 2.3 nM (1SD, n=3) in the deepest water, 12 m above the seafloor. At station 123, located off the coast, TDFe concentrations increased to 24.0 nM at 300 m.

DFe vertical profiles followed the same trend as TDFe ones (**Fig. 3b** and **Table 1**). A maximum was observed in the surface layer, with values of 7.3 and 5.4 nM at stations 122 and 123, respectively and a minimum was reached at 50 m at station 122 with 4.1 nM. At station 122, DFe concentrations also increased close to the sediment, with values reaching 15.2 ± 0.3 nM (1SD, n=3) in the deepest water, 12 m above the seafloor. At station 123, DFe concentrations increased to 3.0 nM below 250 m depth.

Vertical distributions of PFe (**Fig. 3c**) follow the same trend as the DFe and TDFe. At station 122, PFe represents between 73 and 78 % of the total Fe pool except at 50 m where it represented 44 %. The same trend was observed at station 123, with particles representing 76 ± 14 % (n=7) of the total pool except at 50 m where it represented 31 %. The predominance of the particulate phase near continental margin was already observed in numerous studies (Hong and Kester 1986; Johnson et al. 1999; Chase et al. 2005; Lohan and Bruland 2008).

Such TDFe and DFe concentrations are in agreement with previous studies led in coastal areas of the Pacific Ocean. Hong and Kester (1986) observed high total Fe concentrations at coastal stations located near the Peruvian coasts with values reaching 533 nM at 15 m depth. In the benthic boundary layer off Washington and Oregon, Lohan and Bruland (2008) measured labile particulate Fe concentrations (defined by the leaching of the >0.4 µm particulate samples) that reached 162 ± 25 nM. DFe concentrations increased with depth until reaching 50 nM in the bottom water, which was also observed in the same region by Bruland et al. (2005).

At the two shallowest stations, high Fe(II) concentrations were encountered (**Table 1** and **Fig. 3d**). Concentrations increased with depth, reaching maximum bottom values of 7.72 and 16.40 nM at stations 121 and 122 respectively. At station 123, Fe(II) concentrations were lower. A maximum was reached at 300 m ([Fe(II)] = 2.59 nM), where DFe and TDFe

enrichment was also observed. As those depths are in the core of the OMZ, the supply of Fe is probably due to advection from the shelf region. In a recent study Vedamati et al. (2014) also found elevated Fe(II) in bottom waters along transects across continental shelf in the central and southern sectors of the Peruvian coast with the offshore stations of the transects often having a mid water Fe(II) maxima coincident with the secondary nitrite maximum.

Iron isotopes

Vertical profiles of Fe isotopes in the total dissolvable and dissolved pools ($\delta^{56}Fe_{TDFe}$ and $\delta^{56}Fe_{DFe}$, respectively) are plotted in **Fig. 4a and 4b** and data are reported in **Table 1**. For the three stations, either in the total dissolvable or the dissolved pool, values are isotopically light relative to IRMM-14.

For all the stations, a minimum was observed in the surface layer with values ranging from -0.64 ‰ (station 122) to -0.91 ‰ (station 123) in the total dissolvable pool and from -0.68 ‰ (station 122) to -0.97 ‰ (station 123) in the dissolved pool (**Table 1**). Those surface $\delta^{56}Fe$ values are even lighter than values observed below in the water column. Several authors already highlighted light Fe isotopic composition in the surface layer (John and Adkins 2010; Rouxel and Auro 2010; John et al. 2012). However, other studies have also reported heavy compositions (Lacan et al. 2010; Radic et al. 2011). The environment where those stations were located (coastal or open ocean) as well as the sources of Fe and the processes controlling its cycle most likely explain the range of values measured.

Below the surface layer, the distribution of Fe isotopes in the dissolved and the total dissolvable pools is variable but remains light ($\delta^{56}Fe$ from -0.03 to -1.25 ‰). Close to the bottom, the dissolved pool exhibits a minimum (i.e. at station 122) with $\delta^{56}Fe$ values down to -1.25 ‰. Between 187 and 193 m, $\delta^{56}Fe$ values ranged from -1.08 to -1.25 ‰. Such light values at the sediment-water interface have already been highlighted by several authors (Severmann et al. 2006; 2010; John et al. 2012).

At stations 122 and 123, knowing the proportion and the isotopic composition of DFe and TDFe, an Fe isotope budget can be established in order to estimate the isotopic composition of the dissolvable particulate phase, using the following mass balance Equation 1:

$$\delta^{56}Fe_{TDFe} = X_{DFe} * \delta^{56}Fe_{DFe} + X_{PFe} * \delta^{56}Fe_{PFe} \quad \text{(Eq.1)}$$

where X_{DFe} and X_{PFe} are the relative proportion of dissolved and particulate Fe (PFe = TDFe – DFe). Vertical profiles of calculated $\delta^{56}Fe$ values for PFe ($\delta^{56}Fe_{PFe}$) are plotted in **Fig. 4c**

together with uncertainties determined by error propagation using the Monte Carlo (i.e. stochastic simulation) method also reported in **Table 1**. The results show that $\delta^{56}Fe_{PFe}$ values are all isotopically light within uncertainties. At station 122, $\delta^{56}Fe_{PFe}$ values range from -0.63 ± 0.10 ‰ (10 m) to -0.29 ± 0.12 ‰ (193 m) and at station 123, they are in the range of -0.87 ± 0.91 ‰ (20 m) to +0.02 ± 0.20 ‰ (120 m). The Fe isotope fractionation between dissolved and particulate Fe pool, defined as $\Delta\delta^{56}Fe_{PFe\text{-}DFe} = \delta^{56}Fe_{PFe} - \delta^{56}Fe_{DFe}$ is positive within errors (**Fig. 4d** and **Table 1**), with values ranging from +0.05 ± 0.15 ‰ (10 m, Station 122) to +0.96 ± 0.18 ‰ (193 m, station 122). Due to low concentrations of PFe in several samples at Station 122 (50 m) and Station 123 (50, 200 m), $\Delta\delta^{56}Fe_{PFe\text{-}DFe}$ values could not be calculated accurately after error propagation (**Table 1**). Those samples will not be including in the later discussion pertaining to particulate Fe pool.

5. Discussion

5.1. Surface waters

Several sources could explain the Fe enrichment in DFe and TDFe observed in the surface layer at stations 121 and 122. First, atmospheric deposition and riverine inputs are commonly considered the dominant surface sources of Fe in coastal areas (Jickells et al. 2005). It has been shown that aerosols display $\delta^{56}Fe$ values indistinguishable from the crustal value defined as ~0.09 ‰ (Beard et al. 2003b; Waeles et al. 2007). Hence, the light $\delta^{56}Fe$ values observed for TDFe at our three stations (**Table 1**) suggest that dust deposition cannot explain light $\delta^{56}Fe$ values. For comparison, DFe isotope composition in the North Atlantic, a typical region with high dust deposition, yields relatively homogeneous and heavy $\delta^{56}Fe$ values throughout the water column (between +0.30 to +0.45 ‰) (John et al. 2012). It has been demonstrated that Fe delivered from aeolian dust flux accounts for less than a few percent of the Fe required for the observed productivity in the Peru upwelling regime (Fung et al. 2000; Bruland et al. 2005). Considering further the south-eastern trade winds observed in this area (Fung et al., 2000), we suggest that the observed Fe enrichment in surface water is not related to dust deposition.

Total Fe carried by rivers, including both dissolved and suspended fractions, has variable $\delta^{56}Fe$ values ranging essentially from +0.5 to -1 ‰ suggesting that riverine input may, in some cases, be characterized by isotopically light $\delta^{56}Fe$ values relative to igneous rocks (Fantle and DePaolo 2004; Bergquist and Boyle 2006; Escoube et al. 2009; Schroth et

al. 2011; Poitrasson et al. 2014). The largest river draining to the Pacific in South America, the Guayas River and the Guayaquil estuary in Ecuador, are located about 350 km north from Station 121 and 450 km from Stations 122 and 123. Minor freshwater input between 5° and 6°S include the Chira and Sechura-Piura rivers draining terrains of the northern desert of Peru. Although this area was in a la Niña or ENSO-neutral stage at the time the samples were collected, the salinity profiles at the three stations (**Fig. 2**) indicate that there is no freshwater input in surface water, either from river or groundwater input. Hence, it is unlikely that freshwater input could explain the light $\delta^{56}Fe$ values of surface water that are observed in all stations.

Other mechanisms may potentially explain the light values observed in both particulate and dissolved Fe pools. In the surface layer, heterotroph bacteria are known to produce low-molecular weight ferric-specific chelators (siderophores) in Fe-depleted marine environments (Wilhelm and Trick 1994) that allow the dissolution of Fe oxyhydroxide and lithogenic particles. Hence, Fe isotope fractionation in surface seawater can potentially be attributed to Fe-organic ligand complexation and non-congruent dust dissolution, as recently suggested by Conway and John (2014). Experimental determination of the equilibrium isotope fractionation factor between Fe(III) bound to siderophore and the dissolved inorganic Fe complex suggest enrichment in heavier Fe isotopes in the organic complexes (Dideriksen et al. 2008; Morgan et al. 2010), which is opposite of the measured $\delta^{56}Fe_{DFe}$ in the Peruvian system (**Fig. 4**). Another potential mechanism explaining light $\delta^{56}Fe_{DFe}$ values in the surface layer is from biological fractionation processes as previously suggested by de Jong et al. (2007). In the Bothnian Sea, Staubwasser et al. (2013) explained heavier surface $\delta^{56}Fe_{DFe}$ values by biological uptake due to the presence of a cyanobacterial bloom, and in the Equatorial Pacific Ocean, Radic et al. (2013) hypothesized that phytoplankton would favor the uptake of light Fe isotopes and that the surrounding waters would get heavier as they get depleted. In the Peru upwelling regime, large diatoms tend to dominate the biomass in phytoplankton blooms that develop (Wilkerson et al. 2000; Bruland et al. 2005). Those diatom communities could thus play an important role in controlling the Fe isotope fractionation between dissolved and particulate pools.

Despite the current limited knowledge of the biogeochemical processes affecting Fe isotopes in seawater, simple isotopic mass balance consideration between DFe and TDFe suggests that the overall source of Fe to the upper ocean in all stations is isotopically light. As shown in **Fig. 4d**, $\Delta\delta^{56}Fe_{PFe\text{-}DFe}$ values at 10-20 m depth for Stations 122 and 123 are between +0.05 to +0.1 ‰, thus identical within uncertainty. The lack of Fe isotope fractionation

between dissolved and particulate Fe in the upper water column also preclude the identification of potential Fe isotope fractionation through photochemical reactions. Fe(II) concentrations in surface waters were 0.24, 0.59 and 1.05 nM at stations 121, 122 and 123 respectively. Such concentrations could be reached with photoredox cycling of particulate phases. Indeed, previous studies showed that photoreduction of Fe(III) (oxyhydroxides, colloids and particles) and photolysis of organic, colloidal and particulate Fe are processes that occur in surface water (Waite and Morel 1984; Kuma et al. 1992; Barbeau et al. 2001; Rijkenberg et al. 2006; Croot et al. 2008). Wiederhold et al. (2006) observed that Fe isotopes are fractionated during reductive dissolution of Fe oxides promoted by photochemical processes. Enrichment of light isotopes in the dissolved phase was observed.

Based on our current understanding of Fe isotope fractionation both photoreduction and ligand-promoted dissolution could explain the low $\delta^{56}Fe_{DFe}$ values measured in the surface waters but not in the particulate pool (**Table 1**). We propose that the most plausible explanation for both light and similar $\delta^{56}Fe_{PFe}$ and $\delta^{56}Fe_{DFe}$ in the surface layer is the advection and transport of isotopically light Fe from shallower near-shore sediments. The light $\delta^{56}Fe_{PFe}$ values measured in the Baltic Sea were hypothesized to come from water diffusing up from the basin margin sediments after suboxic early-diagenetic remineralization (Gelting et al. 2010; Staubwasser et al. 2013). Along the Peru margin, water masses within the OMZ show a significant enrichment in Fe(II) which may be later oxidized to Fe(III) as it is upwelled or laterally transported within oxygenated surface waters. This freshly formed Fe(III) pool would then record the light signature of Fe(II) when reaching the surface, explaining the light isotopic signature observed in the PFe pool. Processes arising in benthic zone or in intermediate water masses can thus have an impact on the isotopic composition observed in surface waters, as explained in paragraph 5.3 below, using a simple isotopic model.

5.2. Benthic source

In coastal environments, sediments are an important source of Fe to the water column (Hutchins and Bruland 1998; Elrod et al. 2004). Along the Peruvian coasts, low levels of dissolved oxygen increase the rate of benthic fluxes and the amount of Fe(II) escaping from the sediments. At the bottom of station 122, the DFe pool is dominated by Fe(II) (**Table 1**) (between 81 – 100 %) and reaches 15 nM, which is a typical benthic value of hypoxic conditions over the continental shelf (Lohan and Bruland 2008). To our knowledge, it is the first time that the redox speciation was determined at the same time as the isotopic

composition in the water column. Our results clearly indicate that isotopically light DFe between -0.5 to -1.2 ‰ released from the Peruvian margin is almost entirely in the form of Fe(II), with Fe(II)/DFe above 0.8.

Several techniques have previously been used to determine the isotopic signature of the Fe originated from the sediment: porewater measurements, benthic chamber measurements or model (Severmann et al. 2006; 2010; John et al. 2012). In all those studies, an isotopically light δ^{56}Fe signature of the sedimentary dissolved Fe of around -3 ‰ near the sediment-water interface has been determined. Biotic processes involving redox changes are thought to explain the largest Fe isotope fractionations observed in marine sediment porewaters (Johnson et al. 2008). Among those processes, reduction of Fe(III) by dissimilatory Fe-reducing bacteria (process known as dissimilatory iron reduction "DIR") is considered to be responsible for large shifts in isotope compositions (down to -3 ‰) (Crosby et al. 2007; Homoky et al. 2009). However, other mechanisms such as indirect reduction of Fe(III) by sulfide from microbial sulfate reduction, isotopic re-equilibration between Fe(II) and Fe(III) near the sediment-water interface, and partial Fe(II) re-oxidation may also combine to produce such light isotopic values of benthic Fe(II) fluxes (Severmann et al., 2010; Rouxel et al., 2008b; John et al., 2012). In particular, John et al. (2012) suggested that the invariance in dissolved δ^{56}Fe measured by different techniques reflect a single process (rapid Fe(II)-Fe-(III) isotopic equilibration) setting a characteristically light δ^{56}Fe values for the flux from all reducing continental margin sediment. Hence, it can be considered that abiotic Fe redox cycling may contribute to most of Fe isotope fractionation. Regardless of the mechanisms of Fe isotope fractionation, our results confirm the existence of an isotopically light benthic Fe source.

The lowest $\delta^{56}Fe_{DFe}$ values (-1.16 ± 0.09 ‰, 1SD, n=3) found in the deepest water at Station 122, 12 m above the seafloor are in the same range as those measured in the San Pedro basin (from -1.1 to -1.8 ‰) (John et al. 2012) but higher than the mean values ~-3 ‰ reported by (Severmann et al. 2010) for DFe at the sediment/water interface. As shown in **Fig. 5a**, the δ^{56}Fe values for Fe(II) (i.e. when Fe(II)/DFe ≈ 1) estimated at Station 123 is about -0.5 ‰. The results suggest either (i) a substantial variation of the end-member isotopic composition of Fe(II) released from the sediments in our study area, for example due to the development of sulfidic conditions in the surface sediment driving the porewater isotope composition to heavier values (Severmann et al., 2006; Roy et al., 2012); (ii) the isotopic composition of DFe (and Fe(II)) released from sediments has been modified during its advection off-shore.

Regardless of the processes controlling the supply and Fe isotope signatures from benthic sediments, the data also point out the importance of water-column processes affecting Fe signatures of the dissolved and particulate pool, as discussed below. An important observation is that Fe isotopic composition of particles associated with isotopically light Fe(II) is heavier, yielding systematically positive $\Delta\delta^{56}Fe_{PFe\text{-}DFe}$ values up to +0.96 ± 0.18 ‰ in the suboxic water column. The maximum enrichment in heavy Fe isotopes in the particulate Fe pool is observed for the maximum Fe(II) enrichment at depth, which is consistent with redox-driven Fe isotope fractionation. It is now widely reported, both theoretically and experimentally, that partial Fe(II) oxidation produces isotopically heavy Fe(III) oxides (e.g. Bullen et al., 2001; Welch et al., 2003; Dauphas and Rouxel, 2006; Wu et al., 2011b). A maximum $\Delta\delta^{56}Fe_{PFe\text{-}DFe}$ values of about +0.96 ‰ is similar to Fe isotope fractionation during Fe(II) oxidation and precipitation of ferrihydrite (Bullen et al. 2001), but lower than predicted dissolved Fe(III)-Fe(II) equilibrium isotope effect of 3.4 ‰ at 6.5°C (Welch et al. 2003). Additional experimental work has also determined the equilibrium Fe isotope fractionation factors between Fe(III) hydrous oxide and Fe(II)aq of up to 3.2 ‰ (Wu et al. 2011b) reflecting fundamental differences in bonding environments and/or kinetic isotopic effects during natural ferrihydrite precipitation. Adsorption of isotopically heavier Fe (Icopini et al. 2004; Teutsch et al. 2005) onto Fe(III) particles and close vs. open system behaviour during oxidative Fe precipitation may also affect observed $\Delta\delta^{56}Fe_{PFe\text{-}DFe}$ values (Dauphas and Rouxel 2006). In all cases, the sign of $\Delta\delta^{56}Fe_{PFe\text{-}DFe} > 0$‰ is opposite to the isotope fractionation found between dissolved and particulate Fe in the suboxic part of the water column in the Baltic Sea, Eastern Gotland Basin (Staubwasser et al., 2013). Together with previous studies of Fe isotope fractionation during Fe(II) oxidation in subterranean estuaries (Rouxel et al., 2008b), our result suggest that ferrihydrite precipitation should lead to the enrichment in heavy isotopes relative to Fe(II) in marine environments, with a range of fractionation factors controlled by isotope exchange kinetics and mineral phases.

As shown in **Fig. 5b**, $\Delta\delta^{56}Fe_{PFe\text{-}DFe}$ values are correlated with Fe(II)/PFe ratios over the entire profile for Station 122 and 123. This suggests a strong relationship between the relative amount of Fe(II) oxidized in the water column and Fe isotope composition. A preliminary Fe isotope model is presented below.

5.3. Chemical modeling of Fe speciation and isotope composition

DFe in seawater, which is operationally defined as Fe that passes through a 0.2 µm or

0.45 µm filter, can be composed of several pools of Fe that are interacting with each other. A schematic presentation of such Fe pools together with major biogeochemical processes is presented in **Fig. 6**. The predominant form of DFe, noted as DFe(III)-L, is Fe(III) strongly bound to organic ligands (Rue and Bruland 1995). DFe generally includes organic and inorganic colloidal forms of Fe (i.e. size range between 0.02 µm to 0.2 µm), which may represent up to 80 to 90 % of DFe in near-surface waters and 30 to 70 % in deep water, the remainder being defined as truly soluble Fe (Wu et al. 2001). As discussed above, DFe in OMZ such as the Peru margin may also be composed of Fe(II) (referred as DFe(II)) (Millero and Sotolongo 1989; Croot et al. 2001; Lohan and Bruland 2008) which can itself be stabilized by organic ligands. The large range of Fe(II)/DFe ratios obtained in the water column of the Peru margin (**Fig. 7**), from <0.1 to nearly 1, together with high DFe concentrations suggests that all of these pools are present. Similarly, PFe may include several pools of Fe, including biogenic (e.g. planktonic organisms, organic debris and fecal pellets) and inorganic matter (e.g. lithogenic particles). For simplicity, these particulate pools are not distinguished here and are noted as $PFe_{Lith\text{-}Bio}$. In the case of Fe(II)-rich water, PFe may also contain newly precipitated Fe(III) formed after Fe(II) oxidation and colloid precipitation. This pool is referred to as PFe(III). All these forms interact through numerous processes such as biological uptake and degradation, adsorption/desorption reactions, precipitation/dissolution and redox changes, as detailed in **Fig. 6**. Hence, the Fe isotope composition of DFe and PFe will be controlled by the relative contributions of those different pools (i.e. source effects) and biogeochemical processes in the water column.

Presumably, the upward decrease of Fe(II)/DFe throughout the water column (**Fig. 7**) is best explained by a partial oxidation of Fe(II) during upwelling and /or lateral advection. To test this hypothesis, we set up a simple isotopic model that includes: (1) isotopic mass balance between the different dissolved and particulate Fe pools and (2) Fe isotope fractionation during Fe(II) oxidation. This model is aimed to evaluate the importance of Fe(II) vs Fe(III) species in affecting Fe-isotope composition of both the dissolved and particulate Fe pools.

This translates into several equations (in addition to Eq. 1 defined above), assuming that all DFe present in the oxidized form is bound to organic ligands L:

$$DFe^{*}\ \delta^{56}Fe_{DFe} = Fe(II)^{*}\ \delta^{56}Fe_{Fe(II)} + Fe(III)\text{-}L^{*}\ \delta^{56}Fe_{Fe(III)\text{-}L} \qquad \text{(Eq.2)}$$

$$PFe^{*}\ \delta^{56}Fe_{PFe} = PFe(III)^{*}\ \delta^{56}Fe_{PFe(III)} + PFe_{Lith\text{-}Bio}^{*}\ \delta^{56}Fe_{Lith\text{-}Bio} \qquad \text{(Eq.3)}$$

Total Fe(III) is therefore considered to be distributed in the particulate (PFe(III)) and dissolved (Fe(III)-L) pools, as illustrated in **Fig. 6**, such as:

$$Fe(III) = Fe(III)\text{-}L + PFe(III) \quad \text{(Eq.4)}$$

$$TFe = DFe + PFe \quad \text{(Eq.5)}$$

$$DFe = Fe(II) + Fe(III)\text{-}L \quad \text{(Eq.6)}$$

$$PFe = PFe(III) + PFe_{Lith\text{-}Bio} \quad \text{(Eq.7)}$$

The Fe isotope composition of Fe(II) is determined by the proportion *f* of initial Fe(II) pool being oxidized (i.e. Fe(II)/(Fe(II)+Fe(III))), such as:

$$\delta^{56}Fe_{Fe(II)} = \delta^{56}Fe_{Fe(II)ini} + 1000*(\alpha_x - 1)*\ln(f) \quad \text{(Eq.8)}$$

In addition, $\delta^{56}Fe_{Fe(III)} = \delta^{56}Fe_{Fe(III)\text{-}L} * Fe(III)\text{-}L/Fe(III) + \delta^{56}Fe_{PFe(III)} * PFe(III)/Fe(III) = 1000*(\alpha_x - 1) - \delta^{56}Fe_{Fe(II)}$ (Eq.9)

with $\delta^{56}Fe_{Fe(II)ini}$ the Fe isotope composition of the initial pool of Fe(II) and α_x the Fe isotope fractionation factor during Fe(II) oxidation to Fe(III). Finally, the fractionation factor between Fe(III)-L and PFe(III) has been defined as α_L.

As a first approximation, we run the model without the contribution of biogenic (Fe_{Bio}) or lithogenic (Fe_{Lith}) in the particulate Fe pools considering the high concentration of initial Fe(II) in the system. In addition, we limited the number of free parameters by assigning a value to several variables, such as the fractionation factors during Fe(II) oxidation, α_x, and between Fe(III)-L and PFe(III), α_L, and the initial Fe isotope composition for Fe(II). The only parameter that cannot be *a priori* defined is the composition of the Fe(III) pool in Eq. 4, i.e., the fraction of Fe(III)-L vs. PFe(III).

Data for both α_x and α_L have been assigned using previously published experimental data. First, as discussed above, a value of $\alpha_x = 1.001$ has been used since it is consistent with both experimental results obtained by Bullen et al. (2001) during Fe(II) oxidation to goethite and maximum $\Delta\delta^{56}Fe_{PFe\text{-}DFe}$ values measured in our samples. Secondly, a value of $\alpha_L = 0.9995$ has been used to be consistent with the preferential partitioning of light Fe isotopes in organically bound Fe as determined by Brantley et al. (2004). Since this parameter is not well constrained, we also run the model using $\alpha_L = 1.0$ (i.e. no fractionation).

As presented in **Fig. 8**, the equations (1-9) are solved with a spreadsheet software using the above parameters values and *f* values ranging from 1 to 0. This approach allows calculating $\Delta^{56}Fe_{PFe\text{-}DFe}$ values (as well as Fe isotopes values of the different Fe pools) as a function of Fe(II)/PFe. Although a comprehensive modelling of the data and sensitivity tests is beyond the scope of this paper, we obtained a good fit to the data, in particular for Station

122, with Fe(III)-L / Fe(III) = 0.2 and α_L= 0.9995 (i.e. $\Delta\delta^{56}Fe_{Fe(III)\text{-}L\text{-}PFe(III)}$ = -0.5 ‰) (dashed line in **Fig. 8**) and with Fe(III)-L / Fe(III) = 0.35 and α_L= 1.0 (solid line in **Fig. 8**). The main motivation for modelling $\Delta\delta^{56}Fe_{PFe\text{-}DFe}$ values is that the results are independent of the Fe isotope composition assigned to the initial pool of Fe(II).

The values obtained for Fe(III)-L / Fe(III) ratios ranging from 0.2 to 0.35, suggest that between 20 % to 35 % of Fe(III) produced during Fe(II) oxidation remain in the dissolved Fe pool (at least in the colloidal form), while the remainder precipitates due to the low solubility of Fe(III) in seawater (Liu and Millero 2002). It has previously been suggested that partial oxidation of Fe(II) in seawater (or porewater) may lead to the production of light $\delta^{56}Fe_{DFe}$ values in seawater due to the partitioning of isotopically heavy Fe with Fe(III) precipitates (Rouxel et al., 2005; Rouxel et al., 2008b). Since our model is using a Rayleigh-type distillation model (Equation 8) to determine the Fe isotope composition of Fe(II) and Fe(III), our results are generally consistent with previous studies. However, it appears that even in the low oxygen environments as those encountered in OMZ, a significant fraction of DFe is composed of Fe(III)-L, muting the expression of isotopically light DFe that is expected during Fe(II) partial oxidation following Rayleigh-type isotope fractionation processes.

5.4. Iron isotopes as tracers of lithogenic vs. diagenetic sources and internal redox cycling in the water column

The three stations have contrasting Fe isotopic patterns reflecting both Fe sources and water column processes. At the shallowest station (121), yielding the highest TDFe concentrations (up to 456 nM at 100m), $\delta^{56}Fe_{TDFe}$ is close to the crustal value (0.00 ± 0.04 ‰, 1SD, n=4) below 100 m. This suggests that lithogenic input from the continental plateau is the main source of Fe to the water column. This lithogenic supply is so pronounced that it overwhelms the benthic source of Fe(II) that should be observed in bottom waters. At station 122, TDFe concentrations were one order of magnitude lower than station 121. Therefore, lithogenic inputs were less pronounced at the time of sampling, which explains the deviation of $\delta^{56}Fe_{TDFe}$ relative to crustal value. As DFe, TDFe and Fe(II) concentrations increased with depth and reach their maximum close to the sediment, the effect of benthic Fe source on Fe isotope budget becomes preponderant. In all cases, this benthic source induces a dissolved and a particulate Fe pool enriched in light isotopes. As presented in our model above, physical processes such as diffusion or upwelling of water masses will transport this signature to the

water column above the source, where Fe(II) will undergo partial oxidation, and produce a range of δ^{56}Fe values for both PFe and DFe. The deep station 123 shows a different vertical distribution of DFe and PFe than the two other stations with a maximum in TDFe, DFe and Fe(II) concentrations between 250 and 300 m. Those depths correspond to the core of the OMZ suggesting significant advection of benthic Fe from sediments deeper than those encountered at Station 122.

At Station 123, no Fe isotopic compositions have been obtained for depth below 300 m so we cannot rule out the possibility of a deeper water column processes contributing to light Fe isotopes values below 200 m. Nevertheless, differences in Fe isotope signatures of Fe(II) (i.e. when Fe(II)/DFe > 0.8) of the deeper waters of Stations 122 and 123 suggest that the isotope composition of the reductive benthic Fe fluxes is not unique and may range from about -0.6 ‰ down to -1.2 ‰. Hence, our results bear important implications for the quantification of reductive sedimentary Fe sources to the ocean. Recently, Conway and John (2014) assigned a light end-member value of -2.4 ‰ to Fe released from reductive dissolution of margin sediments, with an overall variation of δ^{56}Fe values between -1.82 to -3.45 ‰ (Homoky et al., 2009, Homoky et al., 2013). In comparison, our estimated δ^{56}Fe values of benthic Fe(II) between -0.6 ‰ and -1.2 ‰ are significantly heavier, suggesting that previous estimates of Fe sources from reductive sedimentary dissolution on the African margin (Conway and John, 2014) may be significantly underestimated.

Our results also bear important implications for the mechanisms of Fe release and transfer within OMZ. Scholtz et al. (2014) recently discussed Fe isotopes systematics from a sediment core transect across the Peru upwelling area, located slightly south of our study area. In contrast to expected results (i.e. transfer of isotopically light Fe to the sediments below the OMZ), heaviest δ^{56}Fe values of the surface sediments coincide with the greatest Fe enrichment. This implies that a fraction of the sediment-derived Fe(II) from within the OMZ is precipitated as Fe oxide inthe relatively oxic water beneath the OMZ. In our study, we systematically obtained positive Fe isotope fractionation factors between DFe and PFe with $\Delta\delta^{56}Fe_{PFe\text{-}TDFe}$ values up to +0.96 ‰ consistent with the oxidative precipitation of Fe(II) in the water column. We also reproduce the relationships between $\Delta\delta^{56}Fe_{PFe\text{-}TDFe}$ and Fe(II)/PFe observed throughout the water column at Stations 122 and 123 through partial oxidation. Hence, our data confirm that heavier δ^{56}Fe values measured below the OMZ (Scholz et al. 2014) are best explained by the partial Fe(II) oxidation and precipitation of isotopically heavy Fe-oxyhydroxides in the water columns. Depending on the initial δ^{56}Fe values for Fe(II) that

could range between -0.6 to -1.2 ‰, the Fe isotope fingerprint of precipitated Fe(III) would encompass a range of values either above or below crustal values.

5. Conclusion

In this study, we determined the Fe isotopic composition of total dissolvable and dissolved Fe in the water column of three stations located in an oxygen minimum zone near the Peruvian coast. This hypoxic environment allowed us to study Fe isotope systematics and the complex and dynamic redox cycle of Fe. Two main characteristics were observed in our water column profiles. Firstly, in the surface layer, as the dissolved and particulate Fe concentrations increase, the δ^{56}Fe decreases to lighter isotope compositions relative to the samples collected deeper in the water column. Upwelling and partial oxidation of Fe from deeper layers as well as horizontal advection of isotopically light Fe may explain such features, though we cannot rule out the potential for photo-reduction and biological uptake to influence the light isotopic values of DFe and PFe we observed in surface waters. More studies in controlled environments are certainly needed to better understand fractionation associated with the uptake of Fe by phytoplankton as well as through photoreduction. Secondly, samples collected closest to the sediment show the lightest isotope composition in the dissolved and the particulate pools (-1.25 and -0.53 ‰ respectively) as well as Fe(II)/DFe ratios between 0.8 to 1, consistent with a major benthic Fe sources that is transferred to the ocean water column. To our knowledge it is the first time Fe isotope measurements were done for DFe occurring dominantly as Fe(II). These observations support the idea that sedimentary Fe reduction fractionates Fe isotopes and produces an isotopically light Fe(II) pool transferred to the ocean water column. Imprint of the benthic iron flux already observed at the sediment-ocean boundary is clearly transferred to the water column, but our results also suggest that it will be further modified through partial Fe oxidation and complex interactions between its labile or colloidal and particulate Fe(III) product. Results from the model developed by John et al. (2012) suggest that continental margins contribute 4-12 % of world ocean dissolved Fe and make the ocean's Fe lighter by -0.08 to -0.26 ‰. However, we obtained δ^{56}Fe values between -0.5 to -1.2 ‰ for the benthic Fe(II) fluxes, which is notably heavier than the end-member value of -2.4 ‰ used by Conway and John (2014), suggesting that the quantification of Fe sources to the North Atlantic remain poorly constrained.

In this study, we demonstrate that Fe isotopic composition in OMZ regions are not only affected by the relative contribution of reductive and non-reductive shelf sediment input but also by seawater-column processes during the transport and oxidation of Fe from the source region to open seawater. Although it is clear that Fe isotopes have great potential to trace and quantify the sources of dissolved Fe to the oceans, our results also prompt for the consideration of biogeochemical processes throughout the water column that could modify initial Fe isotope signatures of the sources. With the assumption of an expansion of the OMZ in the oceans, Fe isotopes should ultimately provide useful tracers to assess the contribution of the reductive benthic Fe flux and its export to the global ocean.

Acknowledgements

We thank the officers and crew of RV Meteor for their help and cooperation during M77-4. Special thanks go to the Chief Scientist Dr Lothar Stramma and to Frank Malien (shipboard Nutrient Analysis) for their help during this expedition. We thank the three anonymous reviewers and AE Silke Severmann for their constructive and detailed comments that significantly improved the manuscript. This work is a contribution to the Sonderforschungsbereich 754 “Climate – Biogeochemistry Interactions in the Tropical Ocean” (www.sfb754.de). Financial support for this work was provided by the Deutsche Forschungsgemeinschaft (DFG) via grants to PLC (SFB754 B5), and by Labex Mer (ANR-10-LABX-19-01), Europole Mer and FP7 (#247837) grants to OJR.

Figure caption

Fig.1: Location of the study area in the southeastern part of the Pacific Ocean and location of the stations (basemap created using the USGS map generator, Coastal and Marine Geology Program).

Fig.2: (a) Temperature-Salinity diagram of the three stations studied covering the range of water depths sampled for Fe analysis (i.e. from surface to 160, 198 and 300 m for stations 121 (triangle), 122 (circle) and 123 (square) respectively), (b) Vertical profiles of dissolved oxygen concentrations (µM) at the three stations 121 (triangle), 122 (circle) and 123 (square).

Fig.3: Vertical profiles of (a) total dissolvable Fe (TDFe), (b) dissolved Fe (DFe), (c) total dissolvable particles (PFe = TDFe – DFe) and (d) Fe(II) concentrations (nM) at stations 121 (triangle), 122 (circle) and 123 (square).

Fig.4: Vertical profiles of Fe isotope compositions in the (a) total dissolvable (TDFe), (b) dissolved (DFe) and (c) total dissolvable particles (PFe) pools at stations 121 (triangle), 122 (circle) and 123 (square) (in ‰). (d) represents the isotope fractionation factor between dissolved and particulate Fe pool defined as $\Delta\delta^{56}Fe_{PFe\text{-}DFe} = \delta\ ^{56}Fe_{PFe} - \delta\ ^{56}Fe_{DFe}$.

Fig.5: The relationship between (a) Fe(II)/DFe and $\delta^{56}Fe_{DFe}$ and between (b) $\Delta\delta^{56}Fe_{PFe\text{-}DFe}$ and the ratio Fe(II)/PFe at stations 122 (circle) and 123 (square).

Fig.6: Simplified schematic interpretation of processes affecting the distribution and exchange of the different physico-chemical forms of Fe in the Peruvian OMZ. For simplicity, the model does not consider lateral advection. Vertical bars are not drawn to scale but thickness gradient is proportional to Fe abundance. The incoming flux of Fe(II) result from the reductive dissolution of sediment. The upward decrease of Fe(II) pool result from both partial Fe(II) oxidation and dilution during upwelling of water to the surface. PFe is partitioning between biogenic, lithogenic and PFe(III) fraction. Dissolved Fe, initially exclusively present under Fe(II) form, may also contain Fe(III) bound to organic ligands (FeIII-L) that formed during partial Fe(II) oxidation. A non-reductive source of DFe from the dissolution of sediments may also contribute to Fe(III)-L and/or Fe(II). Lithogenic PFe derive from sediment resuspension and/or atmospheric deposition.

Fig.7: Vertical distribution of the ratio of Fe(II) over DFe at station 122 (circle) and 123 (square).

Fig.8: Results obtained when running the isotopic model detailed in 5.3. section. Equations (1-9) are solved with a spreadsheet software and *f* values (fraction of Fe(II) oxidized) ranging from 1 to 0. This approaches allows calculating $\Delta^{56}Fe_{PFe\text{-}DFe}$ values (as well as Fe isotopes values of the different Fe pools) as a function of Fe(II)/PFe. We obtained a good fit to the data, in particular for Station 122, with Fe(III)-L / Fe(III) = 0.2 and α_2= 0.9995 (i.e. $\Delta\delta^{56}Fe_{Fe(III)\text{-}L\text{-}PFe(III)}$ = -0.5 ‰) (dashed line) and with Fe(III)-L / Fe(III) = 0.35 and α_2= 1.0 (solid line). The main interest for modelling $\Delta\delta^{56}Fe_{PFe\text{-}DFe}$ values is that the results are independent of the Fe isotope composition assigned to the initial pool of Fe(II).

References

Anderson, M. and F. Morel (1980) Uptake of Fe (II) by a diatom in oxic culture medium. *Mar. Biol. Lett* **1**, 263-268.

Balci, N., T. D. Bullen, K. Witte-Lien, W. C. Shanks, M. Motelica and K. W. Mandernack (2006) Iron isotope fractionation during microbially stimulated Fe(II) oxidation and Fe(III) precipitation. *Geochimica Et Cosmochimica Acta* **70**, 622-639.

Barbeau, K., E. L. Rue, K. W. Bruland and A. Butler (2001) Photochemical cycling of iron in the surface ocean mediated by microbial iron(III)-binding ligands. *Nature* **413**, 409-413.

Beard, B. L., C. M. Johnson, J. L. Skulan, K. H. Nealson, L. Cox and H. Sun (2003a) Application of Fe isotopes to tracing the geochemical and biological cycling of Fe. *Chem. Geol.* **195**, 87-117.

Beard, B. L., C. M. Johnson, K. L. Von Damm and R. L. Poulson (2003b) Iron isotope constraints on Fe cycling and mass balance in oxygenated Earth oceans. *Geology* **31**, 629-632.

Bennett, S. A., E. P. Achterberg, D. P. Connelly, P. J. Statham, G. R. Fones and C. R. German (2008) The distribution and stabilisation of dissolved Fe in deep-sea hydrothermal plumes. *Earth Planet. Sci. Lett.* **270**, 157-167.

Bennett, S. A., O. Rouxel, K. Schmidt, D. Garbe-Schönberg, P. J. Statham and C. R. German (2009) Iron isotope fractionation in a buoyant hydrothermal plume, 5 S Mid-Atlantic Ridge. *Geochim. Cosmochim. Acta* **73**, 5619-5634.

Bergquist, B. A. and E. A. Boyle (2006) Iron isotopes in the Amazon River system: Weathering and transport signatures. *Earth Planet. Sci. Lett.* **248**, 54-68.

Blain, S., B. Queguiner, L. Armand, S. Belviso, B. Bombled, L. Bopp, A. Bowie, C. Brunet, C. Brussaard, F. Carlotti, U. Christaki, A. Corbiere, I. Durand, F. Ebersbach, J. L. Fuda, N. Garcia, L. Gerringa, B. Griffiths, C. Guigue, C. Guillerm, S. Jacquet, C. Jeandel, P. Laan, D. Lefevre, C. Lo Monaco, A. Malits, J. Mosseri, I. Obernosterer, Y. H. Park, M. Picheral, P. Pondaven, T. Remenyi, V. Sandroni, G. Sarthou, N. Savoye, L. Scouarnec, M. Souhaut, D. Thuiller, K. Timmermans, T. Trull, J. Uitz, P. van Beek, M. Veldhuis, D. Vincent, E. Viollier, L. Vong and T. Wagener (2007) Effect of natural iron fertilization on carbon sequestration in the Southern Ocean. *Nature* **446**, 1070-U1071.

Bowie, A. R., A. T. Townsend, D. Lannuzel, T. A. Remenyi and P. van der Merwe (2010) Modern sampling and analytical methods for the determination of trace elements in marine particulate material using magnetic sector inductively coupled plasma-mass spectrometry. *Analytica Chimica Acta* **676**, 15-27.

Boyd, P. and M. Ellwood (2010) The biogeochemical cycle of iron in the ocean. *Nat. Geosci.* **3**, 675-682.

Boyd, P. W., T. Jickells, C. S. Law, S. Blain, E. A. Boyle, K. O. Buesseler, K. H. Coale, J. J. Cullen, H. J. W. de Baar, M. Follows, M. Harvey, C. Lancelot, M. Levasseur, N. P. J. Owens, R. Pollard, R. B. Rivkin, J. Sarmiento, V. Schoemann, V. Smetacek, S. Takeda, A. Tsuda, S. Turner and A. J. Watson (2007) Mesoscale iron enrichment experiments 1993-2005: Synthesis and future directions. *Science* **315**, 612-617.

Boyd, P. W., A. J. Watson, C. S. Law, E. R. Abraham, T. Trull, R. Murdoch, D. C. E. Bakker, A. R. Bowie, K. O. Buesseler, H. Chang, M. Charette, P. Croot, K. Downing, R. Frew, M. Gall, M. Hadfield, J. Hall, M. Harvey, G. Jameson, J. LaRoche, M. Liddicoat, R. Ling, M. T. Maldonado, R. M. McKay, S. Nodder, S. Pickmere, R. Pridmore, S. Rintoul, K. Safi, P. Sutton, R. Strzepek, K. Tanneberger, S. Turner, A. Waite and J.

Zeldis (2000) A mesoscale phytoplankton bloom in the polar Southern Ocean stimulated by iron fertilization. *Nature* **407**, 695-702.

Boyle, E. A., S. John, W. Abouchami, J. F. Adkins, Y. Echegoyen-Sanz, M. Ellwood, A. R. Flegal, K. Fornace, C. Gallon and S. Galer (2012) GEOTRACES IC1 (BATS) contamination-prone trace element isotopes Cd, Fe, Pb, Zn, Cu, and Mo intercalibration. *Limnol. Oceanogr. Methods* **10**, 653-665.

Brantley, S. L., L. J. Liermann, R. L. Guynn, A. Anbar, G. A. Icopini and J. Barling (2004) Fe isotopic fractionation during mineral dissolution with and without bacteria. *Geochim. Cosmochim. Acta* **68**, 3189-3204.

Bruland, K. W., R. P. Franks, G. A. Knauer and J. H. Martin (1979) Sampling and analytical method for the determination of Copper, Cadmium, Zinc, and Nickel at the nanogram per liter level in seawater. *Anal. Chem. Acta* **105**, 233-245.

Bruland, K. W., E. L. Rue, G. J. Smith and G. R. DiTullio (2005) Iron, macronutrients and diatom blooms in the Peru upwelling regime: brown and blue waters of Peru. *Marine Chemistry* **93**, 81-103.

Bucciarelli, E., S. Blain and P. Tréguer (2001) Iron and manganese in the wake of the Kerguelen Islands (Southern Ocean). *Mar. Chem.* **73**, 21-36.

Bullen, T. D., A. F. White, C. W. Childs, D. V. Vivit and M. S. Schulz (2001) Demonstration of significant abiotic iron isotope fractionation in nature. *Geology* **29**, 699-702.

Chase, Z., K. S. Johnson, V. A. Elrod, J. N. Plant, S. E. Fitzwater, L. Pickella and C. M. Sakamotob (2005) Manganese and iron distributions off central California influenced by upwelling and shelf width. *Mar. Chem.* **95**, 235-254.

Coale, K. H., K. S. Johnson, F. P. Chavez, K. O. Buesseler, R. T. Barber, M. A. Brzezinski, W. P. Cochlan, F. J. Millero, P. G. Falkowski, J. E. Bauer, R. H. Wanninkhof, R. M. Kudela, M. A. Altabet, B. E. Hales, T. Takahashi, M. R. Landry, R. R. Bidigare, X. J. Wang, Z. Chase, P. G. Strutton, G. E. Friederich, M. Y. Gorbunov, V. P. Lance, A. K. Hilting, M. R. Hiscock, M. Demarest, W. T. Hiscock, K. F. Sullivan, S. J. Tanner, R. M. Gordon, C. N. Hunter, V. A. Elrod, S. E. Fitzwater, J. L. Jones, S. Tozzi, M. Koblizek, A. E. Roberts, J. Herndon, J. Brewster, N. Ladizinsky, G. Smith, D. Cooper, D. Timothy, S. L. Brown, K. E. Selph, C. C. Sheridan, B. S. Twining and Z. I. Johnson (2004) Southern ocean iron enrichment experiment: Carbon cycling in high- and low-Si waters. *Science* **304**, 408-414.

Conway, T. M. and S. G. John (2014) Quantification of dissolved iron sources to the North Atlantic Ocean. *Nature* **511**, 212-215.

Croal, L. R., C. M. Johnson, B. L. Beard and D. K. Newman (2004) Iron isotope fractionation by Fe(II)-oxidizing photoautotrophic bacteria. *Geochimica et Cosmochimica Acta* **68**, 1227-1242.

Croot, P. L., K. Bluhm, C. Schlosser, P. Streu, E. Breitbarth, R. Frew and M. Van Ardelan (2008) Regeneration of Fe(II) during EIFeX and SOFeX. *Geophysical Research Letters* **35**.

Croot, P. L., A. R. Bowie, R. D. Frew, M. T. Maldonado, J. A. Hall, K. A. Safi, R. J. La, P. W. Boyd and C. S. Law (2001) Retention of dissolved iron and Fe-II in an iron induced Southern Ocean phytoplankton bloom. *Geophys. Res. Lett.* **28**, 3425-3428.

Croot, P. L. and M. I. Heller (2012) The importance of kinetics and redox in the biogeochemical cycling of iron in the surface ocean. *Frontiers in microbiology* **3**.

Croot, P. L. and K. A. Hunter (1998) Trace metal distributions across the continental shelf near Otago Peninsula, New Zealand. *Marine Chemistry* **62**, 185-201.

Crosby, H. A., E. E. Roden, C. M. Johnson and B. L. Beard (2007) The mechanisms of iron isotope fractionation produced during dissimilatory Fe(III) reduction by Shewanella putrefaciens and Geobacter sulfurreducens. *Geobiology* **5**, 169-189.

Cutter, G., P. Anderson, L. Codispoti, P. Croot, R. Francois, M. Lohan, H. Obata and M. R. van der Loeff (2010) Sampling and sample-handling protocols for GEOTRACES Cruises, Tech. rep., GEOTRACES.

Dauphas, N. and O. Rouxel (2006) Mass spectrometry and natural variations of iron isotopes. *Mass Spectrometry Reviews* **25**, 515-550.

de Jong, J., V. Schoemann, J.-L. Tison, S. Becquevort, F. Masson, D. Lannuzel, J. Petit, L. Chou, D. Weis and N. Mattielli (2007) Precise measurement of Fe isotopes in marine samples by multi-collector inductively coupled plasma mass spectrometry (MC-ICP-MS). *Anal. Chim. Acta* **589**, 105-119.

Dideriksen, K., J. A. Baker and S. L. S. Stipp (2008) Equilibrium Fe isotope fractionation between inorganic aqueous Fe(III) and the siderophore complex, Fe(III)-desferrioxamine B. *Earth and Planetary Science Letters* **269**, 280-290.

Elrod, V. A., W. M. Berelson, K. H. Coale and K. S. Johnson (2004) The flux of iron from continental shelf sediments: A missing source for global budgets. *Geophys. Res. Lett.* **31, L12307**, doi:10.1029/2004GL020216, 022004.

Escoube, R., O. J. Rouxel, E. Sholkovitz and O. F. X. Donard (2009) Iron isotope systematics in estuaries: The case of North River, Massachusetts (USA). *Geochimica Et Cosmochimica Acta* **73**, 4045-4059.

Fantle, M. S. and D. J. DePaolo (2004) Iron isotopic fractionation during continental weathering. *Earth Planet. Sci. Lett.* **228**, 547-562.

Fung, I. Y., S. K. Meyn, I. Tegen, S. C. Doney, J. G. John and J. K. B. Bishop (2000) Iron supply and demand in the upper ocean. *Glob. Biogeochem. Cycles* **14**, 281-296.

Gelting, J., E. Breitbarth, B. Stolpe, M. Hassellöv and J. Ingri (2010) Fractionation of iron species and iron isotopes in the Baltic Sea euphotic zone. *Biogeosciences* **7**, 2489-2508.

Gledhill, M. and K. N. Buck (2012) The organic complexation of iron in the marine environment: a review. *The microbial ferrous wheel: iron cycling in terrestrial, freshwater, and marine environments*, 29.

Gledhill, M. and C. M. van den Berg (1994) Determination of complexation of iron (III) with natural organic complexing ligands in seawater using cathodic stripping voltammetry. *Mar. Chem.* **47**, 41-54.

Gonzalez-Davila, M., J. M. Santana-Casiano and F. J. Millero (2005) Oxidation of iron(II) nanomolar with H2O2 in seawater. *Geochimica Et Cosmochimica Acta* **69**, 83-93.

Hansen, H. P. (1999) Determination of oxygen. *in: K. Grasshoff, K.K., and M. Ehrhardt (Ed.), Methods of Seawater Analysis. Verlag Chemie, Weinheim*, 75-89.

Helly, J. J. and L. A. Levin (2004) Global distribution of naturally occurring marine hypoxia on continental margins. *Deep Sea Research Part I: Oceanographic Research Papers* **51**, 1159-1168.

Homoky, W., S. Severmann, R. Mills, P. Statham and G. Fones (2009) Pore-fluid Fe isotopes reflect the extent of benthic Fe redox recycling: Evidence from continental shelf and deep-sea sediments. *Geology* **37**, 751-754.

Homoky, W. B., S. G. John, T. M. Conway and R. A. Mills (2013) Distinct iron isotopic signatures and supply from marine sediment dissolution. *Nat. Commun.* **4**.

Hong, H. and D. R. Kester (1986) Redox state of iron in the offshore waters of Peru. *Limnol. Oceanogr.* **31**, 512-524.

Hutchins, D. A. and K. W. Bruland (1998) Iron-limited diatom growth and Si : N uptake ratios in a coastal upwelling regime. *Nature* **393**, 561-564.

Icopini, G. A., A. D. Anbar, S. S. Ruebush, M. Tien and S. L. Brantley (2004) Iron isotope fractionation during microbial reduction of iron: The importance of adsorption. *Geology* **32**, 205-208.

Jickells, T. D., Z. S. An, K. K. Andersen, A. R. Baker, G. Bergametti, N. Brooks, J. J. Cao, P. W. Boyd, R. A. Duce, K. A. Hunter, H. Kawahata, N. Kubilay, J. laRoche, P. S. Liss, N. Mahowald, J. M. Prospero, A. J. Ridgwell, I. Tegen and R. Torres (2005) Global Iron Connections Between Desert Dust, Ocean Biogeochemistry, and Climate. *Science* **308**, 67-71.

John, S. G. and J. F. Adkins (2010) Analysis of dissolved iron isotopes in seawater. *Marine Chemistry* **119**, 65-76.

John, S. G., J. Mendez, J. Moffett and J. Adkins (2012) The flux of iron and iron isotopes from San Pedro Basin sediments. *Geochimica Et Cosmochimica Acta* **93**, 14-29.

Johnson, C. M., B. L. Beard and E. E. Roden (2008) The iron isotope fingerprints of redox and biogeochemical cycling in modern and ancient Earth. *Annu. Rev. Earth Planet. Sci.* **36**, 457-493.

Johnson, C. M., B. L. Beard, E. E. Roden, D. K. Newman and K. H. Nealson (2004) Isotopic constraints on biological cycling of Fe. *Reviews in Mineralogy and Geochemistry* **55**, 359-408.

Johnson, K. S., F. P. Chavez, V. A. Elrod, S. E. Fitzwater, J. T. Pennington, K. R. Buck and P. M. Walz (2001) The annual cycle of iron and the biological response in central California coastal waters. *Geophysical Research Letters* **28**, 1247-1250.

Johnson, K. S., F. P. Chavez and G. E. Friederich (1999) Continental shelf sediments as a primary source of iron to coastal phytoplankton. *Nature* **398**, 697-700.

Kuma, K., S. Nakabayashi, Y. Suzuki, I. Kudo and K. Matsunaga (1992) Photoreduction of Fe(III) by dissolved organic substances and existence of Fe(II) in seawater during spring blooms. *Mar. Chem.* **37**, 15-27.

Lacan, F., A. Radic, C. Jeandel, F. Poitrasson, G. Sarthou, C. Pradoux and R. Freydier (2008) Measurement of the isotopic composition of dissolved iron in the open ocean. *Geophysical Res. Lett.* **35**, doi:10.1029/2008GL035841.

Lacan, F., A. Radic, M. Labatut, C. Jeandel, F. Poitrasson, G. Sarthou, C. Pradoux, J. Chmeleff and R. Freydier (2010) High-Precision Determination of the Isotopic Composition of Dissolved Iron in Iron Depleted Seawater by Double Spike Multicollector-ICPMS. *Anal Chem* **82**, 7103-7111.

Lam, P. J. and J. K. B. Bishop (2008) The continental margin is a key source of iron to the HNLC North Pacific Ocean. *Geophysical Research Letters* **35**.

Liu, X. W. and F. J. Millero (2002) The solubility of iron in seawater. *Marine Chemistry* **77**, 43-54.

Lohan, M. C., A. M. Aguilar-Islas, R. P. Franks and K. W. Bruland (2005) Determination of iron and copper in seawater at pH 1.7 with a new commercially available chelating resin, NTA Superflow. *Analyt. Chim. Acta* **530**, 121-129.

Lohan, M. C. and K. W. Bruland (2008) Elevated Fe(II) and Dissolved Fe in Hypoxic Shelf Waters off Oregon and Washington: An Enhanced Source of Iron to Coastal Upwelling Regimes. *Environ. Sci. Tech.* **42**, 6462-6468.

Maldonado, M. T. and N. M. Price (2001) Reduction and transport of organically bound iron by *Thalassiosira oceanica* (Bacillariophyceae). *J. Phycol.* **37**, 298-309.

Martin, J. H. and S. E. Fitzwater (1988) Iron deficiency limits phytoplankton growth in the north-east Pacific subarctic. *Nature* **331**, 341-343.

Millero, F. J. (1998) Solubility of Fe(III) in seawater. *Earth Planet. Sci. Lett.* **154**, 323-329.

Millero, F. J. and S. Sotolongo (1989) The oxidation of Fe(II) with H_2O_2 in seawater. *Geochim. Cosmochim. Acta* **53**, 1867-1873.

Millero, F. J., S. Sotolongo and M. Izaguirre (1987) The oxidation kinetics of Fe(II) in seawater. *Geochim. Cosmochim. Acta* **51**, 793-801.

Moore, J. K., S. C. Doney, D. M. Glover and I. Y. Fung (2002) Iron cycling and nutrient limitation patterns in surface waters of the World Ocean. *Deep Sea Res. II* **49**, 463-507.

Morgan, J. L. L., L. E. Wasylenki, J. Nuester and A. D. Anbar (2010) Fe Isotope Fractionation during Equilibration of Fe-Organic Complexes. *Environmental Science & Technology* **44**, 6095-6101.

Nishioka, J., H. Obata and D. Tsumune (2013) Evidence of an extensive spread of hydrothermal dissolved iron in the Indian Ocean. *Earth Planet. Sci. Lett.* **361**, 26-33.

Nishioka, J., T. Ono, H. Saito, K. Sakaoka and T. Yoshimura (2011) Oceanic iron supply mechanisms which support the spring diatom bloom in the Oyashio region, western subarctic Pacific. *J. Geophys. Res.* **116**.

Noffke, A., C. Hensen, S. Sommer, F. Scholz, L. Bohlen, T. Mosch, M. Graco and K. Wallmann (2012) Benthic iron and phosphorus fluxes across the Peruvian oxygen minimum zone. *Limnol. Oceanogr.* **57**, 851.

Pennington, J. T., K. L. Mahoney, V. S. Kuwahara, D. D. Kolber, R. Calienes and F. P. Chavez (2006) Primary production in the eastern tropical Pacific: a review. *Progress in Oceanography* **69**, 285-317.

Poitrasson, F., L. Cruz Vieira, P. Seyler, G. Márcia dos Santos Pinheiro, D. Santos Mulholland, M.-P. Bonnet, J.-M. Martinez, B. Alcantara Lima, G. Resende Boaventura and J. Chmeleff (2014) Iron isotope composition of the bulk waters and sediments from the Amazon River Basin. *Chem. Geol.* **377**, 1-11.

Pollard, R. T., I. Salter, R. J. Sanders, M. I. Lucas, C. M. Moore, R. A. Mills, P. J. Statham, J. T. Allen, A. R. Baker, D. C. E. Bakker, M. A. Charette, S. Fielding, G. R. Fones, M. French, A. E. Hickman, R. J. Holland, J. A. Hughes, T. D. Jickells, R. S. Lampitt, P. J. Morris, F. H. Nedelec, M. Nielsdottir, H. Planquette, E. E. Popova, A. J. Poulton, J. F. Read, S. Seeyave, T. Smith, M. Stinchcombe, S. Taylor, S. Thomalla, H. J. Venables, R. Williamson and M. V. Zubkov (2009) Southern Ocean deep-water carbon export enhanced by natural iron fertilization. *Nature* **457**, 577-U581.

Radic, A., F. Lacan and J. W. Murray (2011) Iron isotopes in the seawater of the equatorial Pacific Ocean: New constraints for the oceanic iron cycle. *Earth and Planetary Science Letters* **306**, 1-10.

Rijkenberg, M. J. A., L. J. A. Gerringa, V. E. Carolus, I. Velzeboer and H. J. W. de Baar (2006) Enhancement and inhibition of iron photoreduction by individual ligands in open ocean seawater. *Geochimica Et Cosmochimica Acta* **70**, 2790-2805.

Rouxel, O. and M. Auro (2010) Iron isotope variations in coastal seawater determined by Multicollector ICP-MS. *Geostandards and Geoanalytical Research* **34**, 135-144.

Rouxel, O., W. C. Shanks, W. Bach and K. J. Edwards (2008a) Integrated Fe- and S-isotope study of seafloor hydrothermal vents at East Pacific rise 9-10 degrees N. *Chemical Geology* **252**, 214-227.

Rouxel, O., E. Sholkovitz, M. Charette and K. J. Edwards (2008b) Iron isotope fractionation in subterranean estuaries. *Geochimica Et Cosmochimica Acta* **72**, 3413-3430.

Roy, M., O. Rouxel, J. B. Martin and J. E. Cable (2012) Iron isotope fractionation in a sulfide-bearing subterranean estuary and its potential influence on oceanic Fe isotope flux. *Chem. Geol.* **300**, 133-142.

Rue, E. L. and K. W. Bruland (1995) Complexation of iron(III) by natural organic ligands in the Central North Pacific as determined by a new competitive ligand equilibration/adsorptive cathodic stripping voltammetric method. *Mar. Chem.* **50**, 117-138.

Santana-Casiano, J. M., M. Gonzaalez-Davila and F. J. Millero (2005) Oxidation of nanomolar levels of Fe(II) with oxygen in natural waters. *Environmental Science & Technology* **39**, 2073-2079.

Sarthou, G., E. Bucciarelli, F. Chever, S. P. Hansard, M. Gonzalez-Davila, J. M. Santana-Casiano, F. Planchon and S. Speich (2011) Labile Fe(II) concentrations in the Atlantic sector of the Southern Ocean along a transect from the subtropical domain to the Weddell Sea Gyre. *Biogeosciences* **8**, 2461-2479.

Scholz, F., S. Severmann, J. McManus and C. Hensen (2014) Beyond the Black Sea paradigm: The sedimentary fingerprint of an open-marine iron shuttle. *Geochim. Cosmochim. Acta* **127**, 368-380.

Schroth, A. W., J. Crusius, F. Chever, B. C. Bostick and O. J. Rouxel (2011) Glacial influence on the geochemistry of riverine iron fluxes to the Gulf of Alaska and effects of deglaciation. *Geophys. Res. Lett.* **38**.

Sell, K. S. and J. W. Morse (2006) Dissolved Fe2+ and Sigma H2S behavior in sediments seasonally overlain by hypoxic-to-anoxic waters as determined by CSV microelectrodes. *Aquatic Geochemistry* **12**, 179-198.

Severmann, S., C. Johnson, B. Beard, C. German, H. Edmonds, H. Chiba and D. Green (2004) The effect of plume processes on the Fe isotope composition of hydrothermally derived Fe in the deep ocean as inferred from the Rainbow vent site, Mid-Atlantic Ridge, 36 14′ N. *Earth Planet. Sci. Lett.* **225**, 63-76.

Severmann, S., C. M. Johnson, B. L. Beard and J. McManus (2006) The effect of early diagenesis on the Fe isotope compositions of porewaters and authigenic minerals in continental margin sediments. *Geochim. Cosmochim. Acta* **70**.

Severmann, S., J. McManus, W. M. Berelson and D. E. Hammond (2010) The continental shelf benthic iron flux and its isotope composition. *Geochim. Cosmochim. Acta* **74**, 3984-4004.

Sharma, M., M. Polizzotto and A. D. Anbar (2001) Iron isotopes in hot springs along the Juan de Fuca Ridge. *Earth Planet. Sci. Lett.* **194**, 39-51.

Staubwasser, M., R. Schoenberg, F. von Blanckenburg, S. Krüger and C. Pohl (2013) Isotope fractionation between dissolved and suspended particulate Fe in the oxic and anoxic water column of the Baltic Sea. *Biogeosciences* **10**, 233-245.

Stramma, L., G. C. Johnson, E. Firing and S. Schmidtko (2010) Eastern Pacific oxygen minimum zones: Supply paths and multidecadal changes. *Journal of Geophysical Research-Oceans* **115**.

Stramma, L., G. C. Johnson, J. Sprintall and V. Mohrholz (2008) Expanding oxygen-minimum zones in the tropical oceans. *Science* **320**, 655-658.

Tagliabue, A., L. Bopp and O. Aumont (2009) Evaluating the importance of atmospheric and sedimentary iron sources to Southern Ocean biogeochemistry. *Geophysical Research Letters* **36**.

Tagliabue, A., L. Bopp, J. C. Dutay, A. R. Bowie, F. Chever, P. Jean-Baptiste, E. Bucciarelli, D. Lannuzel, T. Remenyi, G. Sarthou, O. Aumont, M. Gehlen and C. Jeandel (2010) Hydrothermal contribution to the oceanic dissolved iron inventory. *Nature Geoscience* **3**, 252-256.

Teutsch, N., U. vonGunten, D. Porcelli, O. A. Cirpka and A. N. Halliday (2005) Adsorption as a cause for Iron Isotope fractionation in reduced groundwater. *Geochim. Cosmochim. Acta* **17**, 4175-4185.

Toner, B. M., S. C. Fakra, S. J. Manganini, C. M. Santelli, M. A. Marcus, J. Moffett, O. Rouxel, C. R. German and K. J. Edwards (2009) Preservation of iron(II) by carbon-rich matrices in a hydrothermal plume. *Nature Geoscience* **2**, 197-201.

Vedamati, J., T. Goepfert and J. W. Moffett (2014) Iron speciation in the eastern tropical South Pacific oxygen minimum zone off Peru. *Limnol. Oceanogr* **59**, 1945-1957.

Waeles, M., A. R. Baker, T. Jickells and J. Hoogewerff (2007) Global dust teleconnections: aerosol iron solubility and stable isotope composition. *Environmental Chemistry* **4**, 233-237.

Waite, T. D. and F. M. M. Morel (1984) Photoreductive dissolution of colloidal iron oxides in natural waters. *Env. Sci. Technol.* **18**, 860-868.

Welch, S. A., B. L. Beard, C. M. Johnson and P. S. Braterman (2003) Kinetic and equilibrium Fe isotope fractionation between aqueous Fe(II) and Fe(III). *Geochimica et Cosmochimica Acta* **67**, 4231-4250.

Weyer, S. and J. B. Schwieters (2003) High precision Fe isotope measurements with high mass resolution MC-ICPMS. *International Journal of Mass Spectrometry* **226**, 355-368.

Wiederhold, J. G., S. M. Kraemer, N. Teutsch, P. M. Borer, A. N. Halliday and R. Kretzschmar (2006) Iron isotope fractionation during proton-promoted, ligand-controlled, and reductive dissolution of goethite. *Environ. Sci. Tech.* **40**, 3787-3793.

Wilhelm, S. W. and C. G. Trick (1994) Iron-limited growth in cyanobacteria: Multiple siderophore production is a common response. *Limnol. Oceanogr.* **39**, 1979-1984.

Wilkerson, F. P., R. C. Dugdale, R. M. Kudela and F. P. Chavez (2000) Biomass and productivity in Monterey Bay, California: contribution of the large phytoplankton. *Deep-Sea Res. Part II-Top. Stud. Oceanogr.* **47**, 1003-1022.

Wu, J., E. Boyle, W. Sunda and L.-S. Wen (2001) Soluble and colloidal iron in the Oligotrophic North Atlantic and North Pacific. *Science* **293**, 847-849.

Wu, J. F., M. L. Wells and R. Rember (2011a) Dissolved iron anomaly in the deep tropical-subtropical Pacific: Evidence for long-range transport of hydrothermal iron. *Geochimica Et Cosmochimica Acta* **75**, 460-468.

Wu, L., B. L. Beard, E. E. Roden and C. M. Johnson (2011b) Stable Iron Isotope Fractionation Between Aqueous Fe(II) and Hydrous Ferric Oxide. *Environ. Sci. Tech.* **45**, 1847-1852.

Table 1: Fe(II), DFe, PFe and TDFe concentrations and δ^{56}Fe values in the water column of Stations 121, 122 and 123 from the Peru margin.

Depth (m)	Fe(II) (nM)	DFe (nM)	**δ^{56}Fe DFe**	2SD	TDFe (nM)	**δ^{56}Fe TDFe**	2SD	PFe* (nM)	2SD	**δ^{56}Fe PFe$^{\$}$**	2SD$^{\$}$	FeII/DFe	FeII/TDFe	FeII/PFe	DFe/TDFe	**$\Delta\delta^{56}$Fe* (PFe-DFe)**	2SD
Station 121 (5°10.01' S; 81°21.02' W; 161m water depth																	
10	0.24	-	**-**	-	14.6	**-0.81**	0.06	-		-	-	-	0.02	-	-	-	-
50	0.34	-	**-**	-	115	**-0.24**	0.04	-		-	-	-	0.00	-	-	-	-
100	1.3	-	**-**	-	456	**0.04**	0.04	-		-	-	-	0.00	-	-	-	-
154	6.3	-	**-**	-	201	**0.01**	0.04	-		-	-	-	0.03	-	-	-	-
157	7.0	-	**-**	-	191	**-0.04**	0.04	-		-	-	-	0.04	-	-	-	-
160	7.7	-	**-**	-	197	**-0.03**	0.04	-		-	-	-	0.04	-	-	-	-
Station 122 (6°0.01' S; 81°15.44' W; 198m water depth)																	
10	0.59	7.3	**-0.68**	0.06	32.9	**-0.64**	0.04	25.6	4.0	**-0.63**	0.09	0.08	0.02	0.02	0.22	**0.05**	0.11
50	0.39	4.1	**-0.32**	0.12	7.3	**-0.40**	0.06	3.2	1.1	**-0.51**	0.38	0.09	0.05	0.12	0.56	**-0.19**	0.40
100	1.4	7.8	**-0.83**	0.12	29.2	**-0.54**	0.04	21.4	3.7	**-0.44**	0.15	0.18	0.05	0.06	0.27	**0.39**	0.19
187	12.2	15.0	**-1.08**	0.06	63.4	**-0.52**	0.04	48.4	7.8	**-0.35**	0.11	0.81	0.19	0.25	0.24	**0.73**	0.12
190	16.4	15.4	**-1.15**	0.06	62.8	**-0.58**	0.04	47.3	7.8	**-0.39**	0.08	1.00	0.26	0.35	0.25	**0.76**	0.10
193	14.2	15.0	**-1.25**	0.06	59.2	**-0.53**	0.04	44.1	7.4	**-0.29**	0.09	0.94	0.24	0.32	0.25	**0.96**	0.11
Station 123 (5°59.99' S; 81°30.09' W; 2430m water depth)																	
20	1.05	5.4	**-0.97**	0.12	14.3	**-0.91**	0.06	9.0	2.0	**-0.87**	0.26	0.20	0.07	0.12	0.38	**0.10**	0.29
50	0.83	2.5	**-0.43**	0.12	3.7	**-0.66**	0.12	<DL	-	-	-	-	-	-	-	-	-
80	0.83	1.9	**-0.71**	0.11	7.7	**-0.29**	0.06	5.8	1.0	**-0.15**	0.18	0.43	0.11	0.14	0.25	**0.56**	0.21
120	0.93	2.0	**-0.6**	0.11	7.3	**-0.1**	0.06	5.3	0.9	**0.02**	0.21	0.46	0.13	0.17	0.28	**0.62**	0.24

			0			**5**											
200	1.23	1.9	**-0.31**	0.11	4.4	**-0.21**	0.12	2.5	0.6	**-0.13**	0.42	0.63	0.28	0.50	0.44	**0.18**	0.43
250	2.25	3.0	**-0.66**	0.12	22.8	**-0.36**	0.04	19.8	2.6	**-0.32**	0.09	0.75	0.10	0.11	0.13	**0.34**	0.15
300	2.59	2.8	**-0.47**	0.12	24.0	**-0.34**	0.04	21.2	2.7	**-0.32**	0.07	0.92	0.11	0.12	0.12	**0.15**	0.14

Concentration DFe and PFe data are given with a precision of 10%.

* total dissolvable particles (PFe) have been calculated substracting the DFe to the TDFe. Precision is given

$ Fe isotope composition of PFe has been calculated using isotope mass balance relationships between DFe and PFe. Error (2SD) has been obtained after error propagation

£ Fe isotope fractionation factor D d56Fe* (PFe-DFe) determined as d56Fe PFe - d56Fe DFe

- 'not determined'

<DL : below detection limits

Figure 1

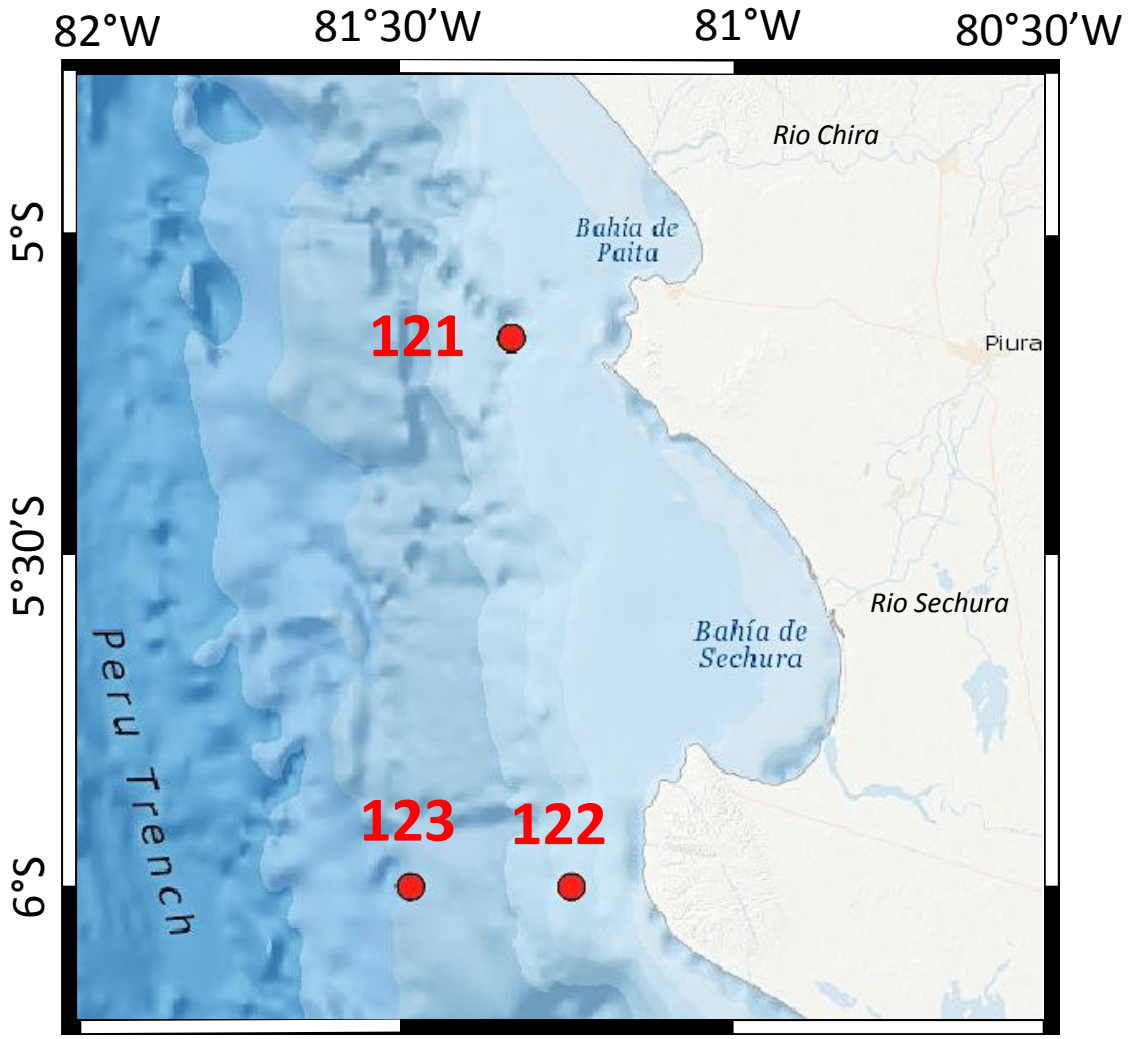

Figure 1

Figure 2

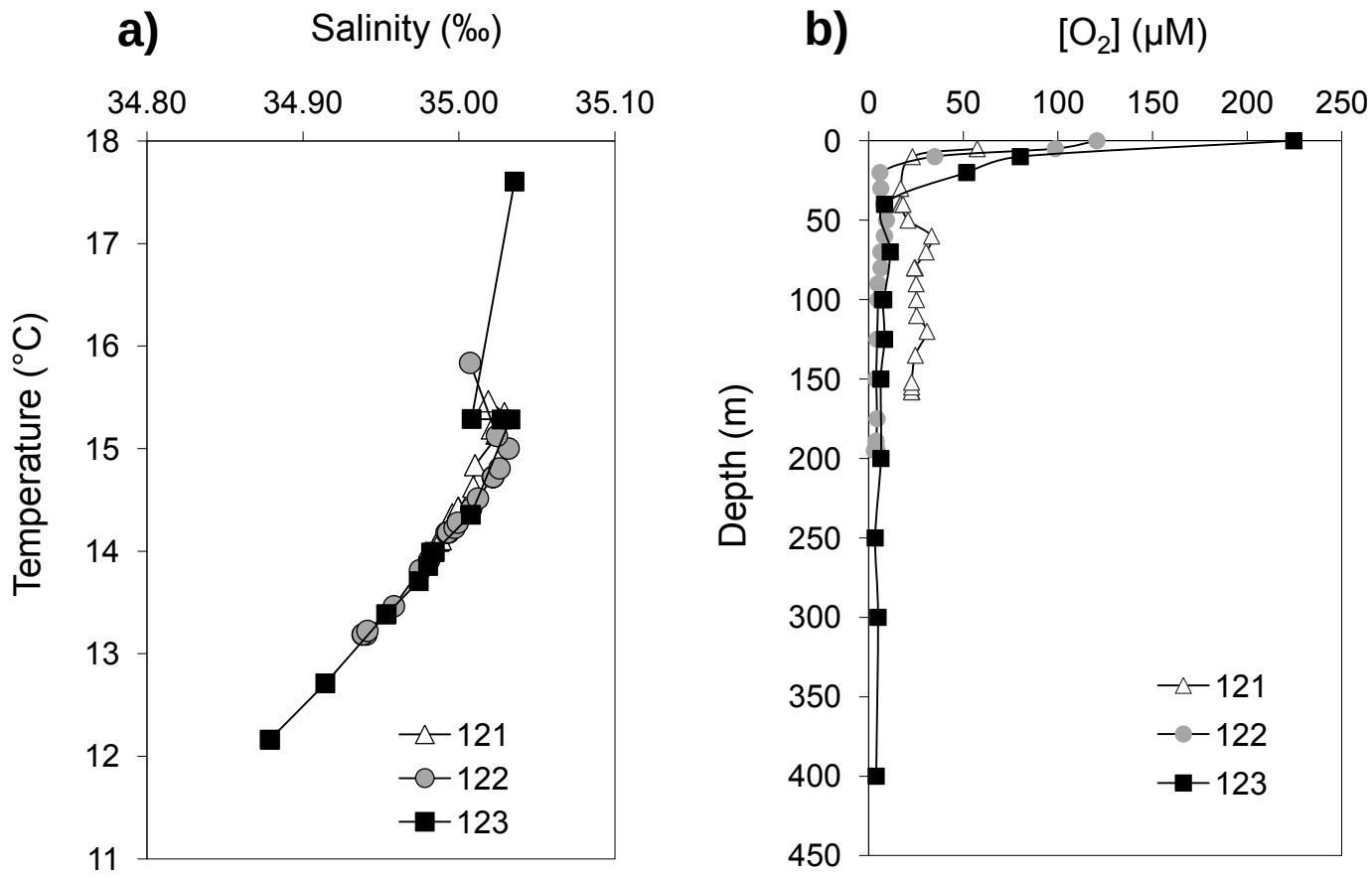

Figure 2

Figure 3

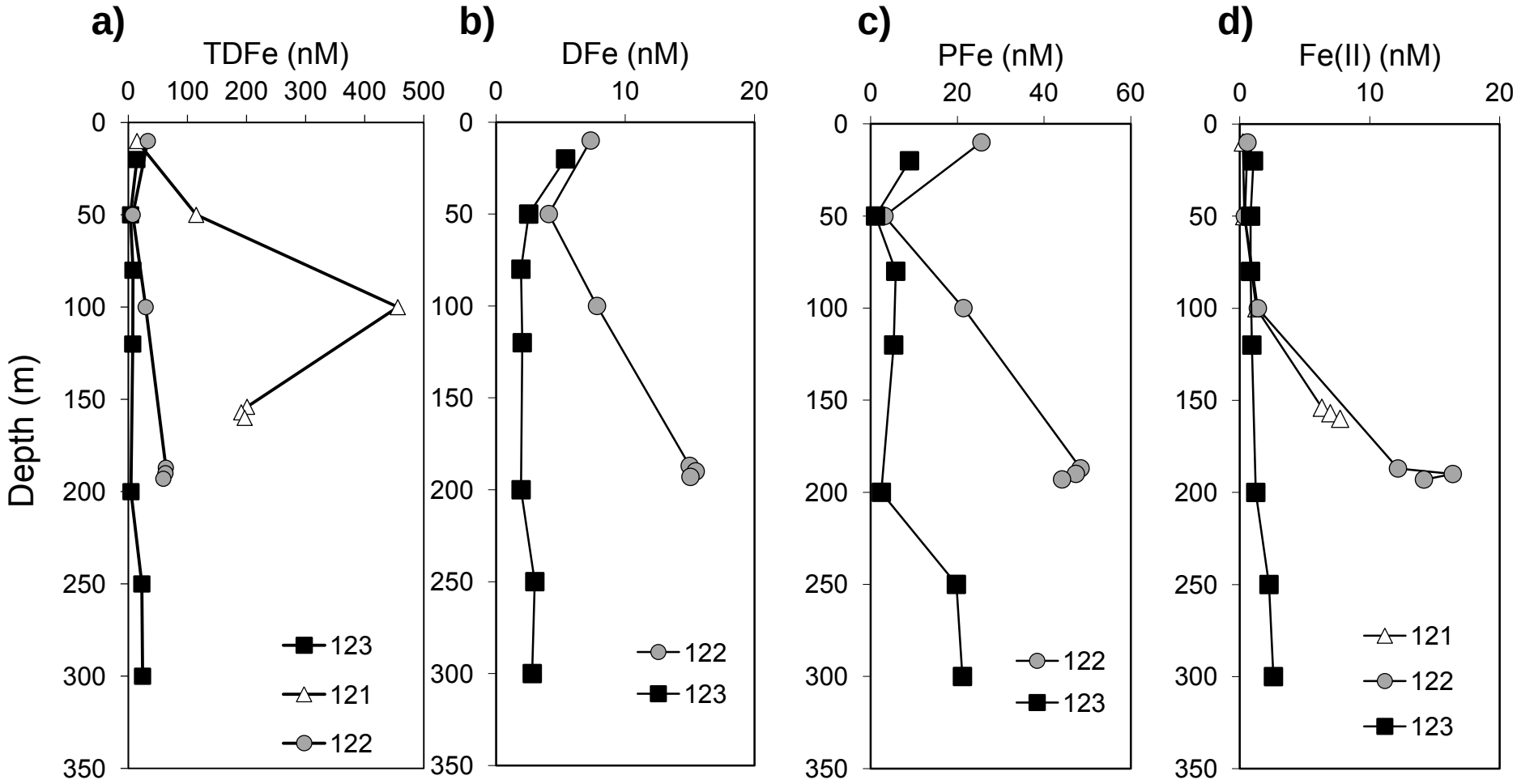

Figure 3

Figure 4

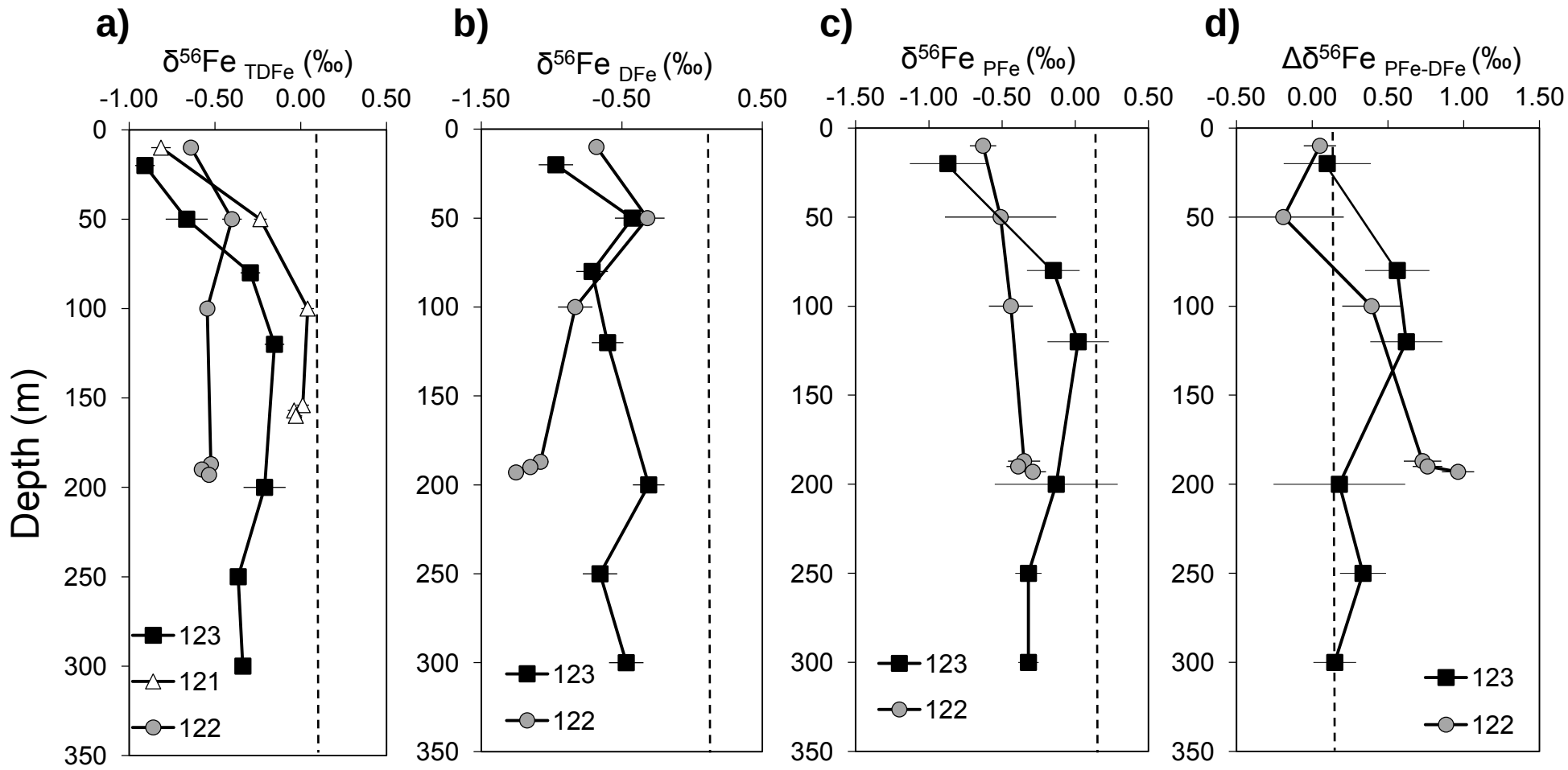

Figure 4

Figure 5

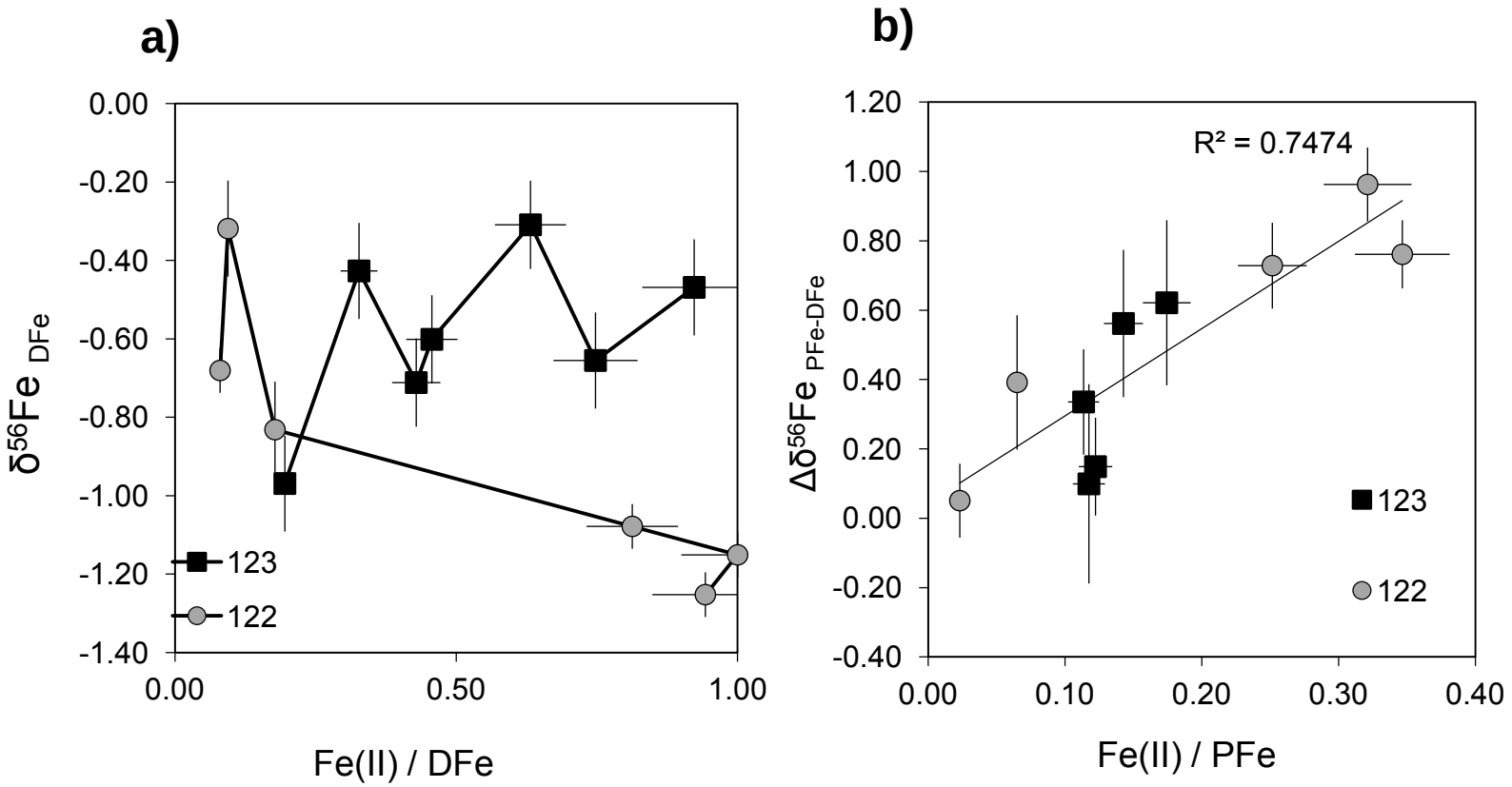

Figure 5

Figure 6

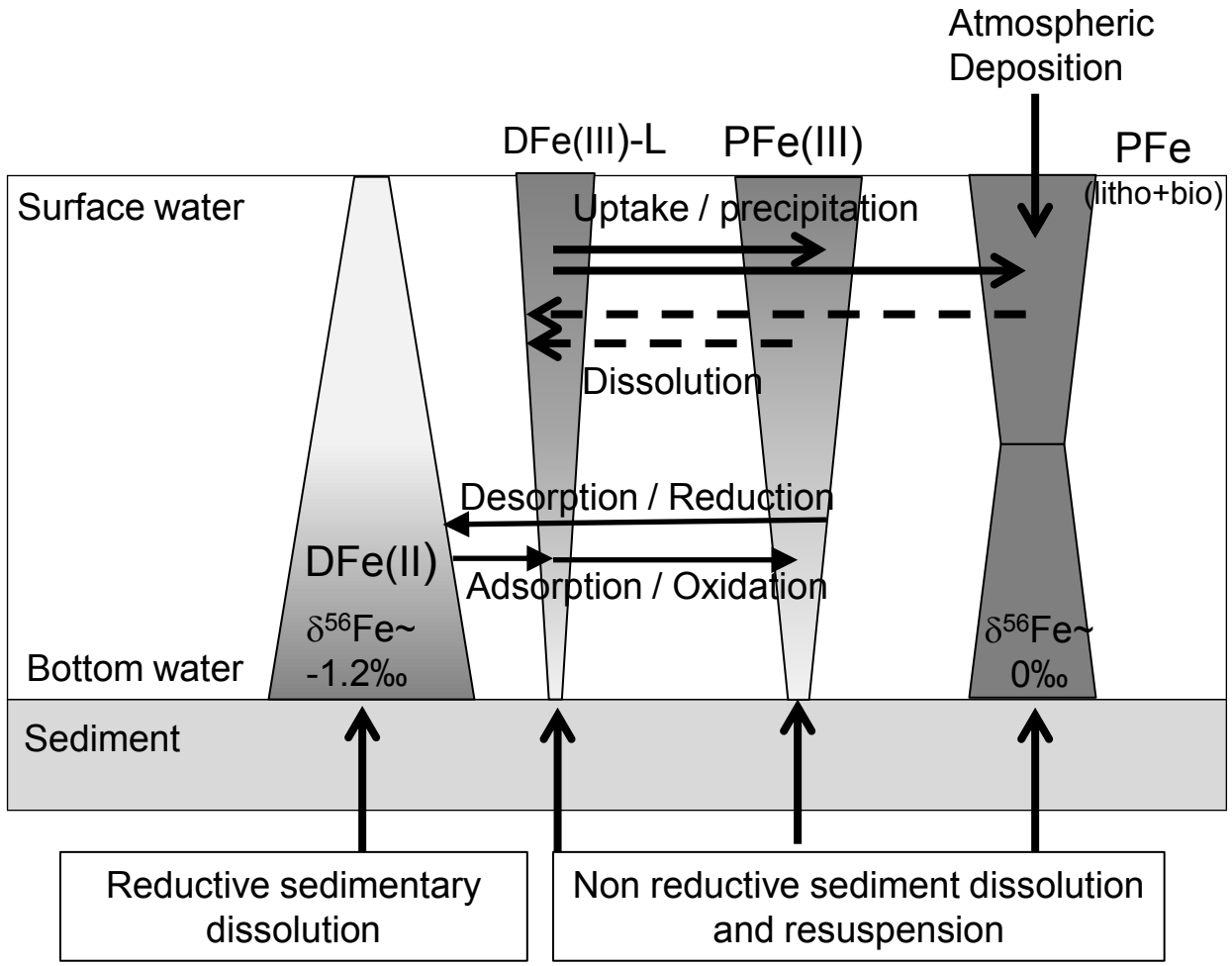

Figure 6

Figure 7

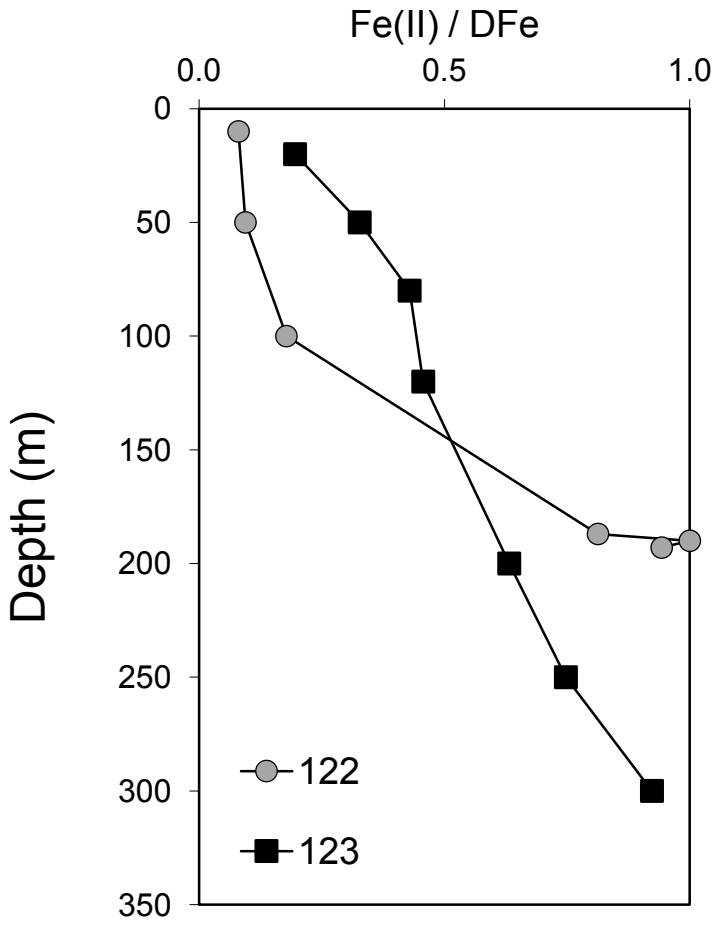

Figure 7

Figure 8

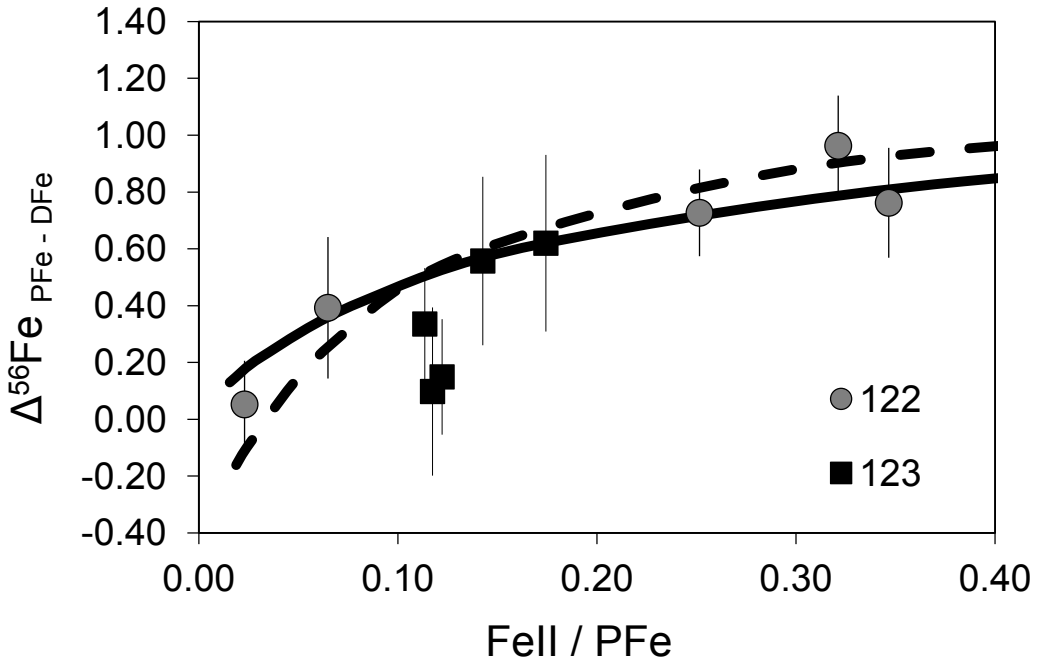

Figure 8